The Meteoritical Society

Meteoritics & Planetary Science 55, Nr 6, 1176–1206 (2020)
doi: 10.1111/maps.13412

The presolar grain inventory of fine-grained chondrule rims in the Mighei-type (CM) chondrites

Jan LEITNER[1]*, Knut METZLER[2], Christian VOLLMER[3], Christine FLOSS[4], Pierre HAENECOUR[4,5], János KODOLÁNYI[1], Dennis HARRIES[6], and Peter HOPPE[1]

[1]Max Planck Institute for Chemistry, Particle Chemistry Department, Hahn-Meitner-Weg 1, 55128 Mainz, Germany
[2]Institute for Planetology, University of Münster, 48149 Münster, Germany
[3]Institute for Mineralogy, University of Münster, 48149 Münster, Germany
[4]Laboratory for Space Sciences, Physics Department and McDonnell Center for Space Sciences, Washington University in St. Louis, One Brookings Drive, St. Louis, Missouri 63130, USA
[5]Present Address: Lunar and Planetary Laboratory, The University of Arizona, 1629 E. University Blvd., Kuiper, Space Science Bldg, Tucson, Arizona 85721-0092, USA
[6]Institute of Geoscience, Friedrich Schiller University Jena, Carl-Zeiss-Promenade 10, 07745 Jena, Germany
*Corresponding author. E-mail: jan.leitner@mpic.de

(Received 27 February 2019; revision accepted 05 October 2019)

Abstract–We investigated the inventory of presolar silicate, oxide, and silicon carbide (SiC) grains of fine-grained chondrule rims in six Mighei-type (CM) carbonaceous chondrites (Banten, Jbilet Winselwan, Maribo, Murchison, Murray, and Yamato 791198), and the CM-related carbonaceous chondrite Sutter's Mill. Sixteen O-anomalous grains (nine silicates, six oxides) were detected, corresponding to a combined matrix-normalized abundance of ~18 ppm, together with 21 presolar SiC grains (~42 ppm). Twelve of the O-rich grains are enriched in ^{17}O, and could originate from low-mass asymptotic giant branch stars. One grain is enriched in ^{17}O and significantly depleted in ^{18}O, indicative of additional cool bottom processing or hot bottom burning in its stellar parent, and three grains are of likely core-collapse supernova origin showing enhanced $^{18}O/^{16}O$ ratios relative to the solar system ratio. We find a presolar silicate/oxide ratio of 1.5, significantly lower than the ratios typically observed for chondritic meteorites. This may indicate a higher degree of aqueous alteration in the studied meteorites, or hint at a heterogeneous distribution of presolar silicates and oxides in the solar nebula. Nevertheless, the low O-anomalous grain abundance is consistent with aqueous alteration occurring in the protosolar nebula and/or on the respective parent bodies. Six O-rich presolar grains were studied by auger electron spectroscopy, revealing two Fe-rich silicates, one forsterite-like Mg-rich silicate, two Al-oxides with spinel-like compositions, and one Fe-(Mg-)oxide. Scanning electron and transmission electron microscopic investigation of a relatively large silicate grain (490 nm × 735 nm) revealed that it was crystalline åkermanite ($Ca_2Mg[Si_2O_7]$) or a an åkermanite-diopside ($MgCaSi_2O_6$) intergrowth.

INTRODUCTION

Primitive meteorites, micrometeorites, interplanetary dust particles (IDPs), and cometary material contain small amounts of refractory dust grains which predate the formation of the Sun and our planetary system and are characterized by highly anomalous isotopic compositions that cannot be explained by chemical or physical processes within the solar system (e.g., Zinner 2014). Instead, they possess nucleosynthetic signatures of their stellar parents. These presolar or "stardust" grains condensed in the ejecta of evolved stars or stellar explosions (novae and supernovae). Subsequently, they became part of the interstellar medium (ISM) where they were exposed to high-energetic irradiation, exposure to shockwaves from nearby supernova

explosions, and grain–grain collisions. The presolar dust that is found today in primitive solar system materials mostly escaped alteration and homogenization processes in the ISM as well as during the formation of the protosolar nebula and protoplanetary disk (e.g., Zinner 2014). The properties of these grains hold valuable information on stellar nucleosynthesis and evolution, grain formation in circumstellar environments, and the types of stars contributing material to the nascent solar system. Moreover, determining the abundances and distributions of the different types of presolar dust allows for the study of parent body alteration processes, and also potential heterogeneities in the distribution of presolar circumstellar matter within the nascent solar system (Zinner 2014; Floss and Haenecour 2016).

Silicates are the most abundant presolar grain species large enough for the isotopic analysis of single grains (e.g., Floss and Haenecour 2016). In contrast to the more refractory types of presolar dust (silicon carbide, graphite, Si_3N_4, oxides), silicates cannot be separated chemically from their host meteorites (Nguyen and Zinner 2004). Instead, they have to be analyzed in situ or among physically separated matrix grains with high spatial resolution techniques like NanoSIMS (nanoscale secondary ion mass spectrometry) ion imaging (e.g., Hoppe et al. 2013). Matrix-normalized presolar silicate abundances can exceed 200 parts per million (ppm) in the most primitive unequilibrated meteorites (e.g., Nittler et al. 2018). Oxide stardust grains are generally less abundant, with concentrations of up to tens of ppm in meteorites (Vollmer et al. 2009; Leitner et al. 2012a; Haenecour et al. 2018), and abundances of presolar silicon carbide (SiC) are typically in the range of tens of ppm in primitive meteorites (Floss and Stadermann 2009b; Nguyen et al. 2010; Leitner et al. 2012a, 2018; Zhao et al. 2013, 2014; Davidson et al. 2014a).

According to their oxygen isotopic compositions, presolar silicate and oxide grains are divided into four distinct groups (Nittler et al. 1997, 2008). Most of these grains (>85%) belong to Groups 1 and 2. Grains of Group 1 have higher than solar system $^{17}O/^{16}O$ (0.41–5×10^{-3}) and close to or lower than solar system $^{18}O/^{16}O$ ratios (1–2×10^{-3}), compatible with low-mass AGB star origins. However, a recent investigation of Mg isotopes revealed several Group 1 silicates with large enrichments of ^{25}Mg, indicative of explosive H-burning, refuting a low-mass origin for these grains (Leitner and Hoppe 2019; Nittler 2019; Verdier-Paoletti et al. 2019b). Group 2 grains are characterized by less pronounced enrichments of ^{17}O relative to the solar system composition than the Group 1 grains ($\leq 1.7 \times 10^{-3}$) and by significant depletions of ^{18}O ($^{18}O/^{16}O$ $<\sim 0.8 \times 10^{-3}$, although $< 1 \times 10^{-3}$ is often applied as criterion). Proposed origins include 1.2–1.8 $M_\odot$ AGB stars of subsolar metallicity (the metallicity Z denotes the mass fraction of elements heavier than helium) that experienced additional mixing processes, like cool bottom processing (CBP) in RGB and AGB stars with $M < 1.5\ M_\odot$ (Wasserburg et al. 1995; Nollett et al. 2003; Palmerini et al. 2011) and hot-bottom burning (HBB) in intermediate-mass (4–8 $M_\odot$) AGB stars (Lugaro et al. 2017).

Most of the Group 3 grains, with ^{17}O and ^{18}O depletions, might have formed around low-mass (<1.4 $M_\odot$) AGB stars with $Z<Z_\odot$. However, the isotopic compositions of several Group 3 grains could also indicate an origin from core-collapse supernova (CCSN) explosions (Nittler et al. 2008; Nguyen and Messenger 2014; Hoppe et al. 2015). Grains of Group 4 have significantly enhanced $^{18}O/^{16}O$ ratios, with CCSNe as the most probable stellar sources (Nittler et al. 2008; Vollmer et al. 2008; Nguyen and Messenger 2014). A small number of grains (<1%) show extreme enrichments of ^{17}O (>5–6×10^{-3}) that cannot be accounted for by nucleosynthesis in single AGB stars (Nittler et al. 2008; Gyngard et al. 2011; Palmerini et al. 2011). Binary stars experiencing mass transfer are potential sources for these "extreme Group 1" grains (Nittler et al. 2008); some of them could have formed in the ejecta of nova outbursts (Nittler and Hoppe 2005; Nittler et al. 2008, 2012; Gyngard et al. 2010, 2011; Leitner et al. 2012b; Nguyen and Messenger 2014).

Dust condensation around AGB stars occurs almost exclusively during the thermally pulsing (TP-) AGB phase. At the start of the TP-AGB phase, the stellar envelope is oxygen-rich (i.e., $C/O < 1$), facilitating the formation of silicate and oxide stardust. After each thermal pulse, material from the He-intershell dominated by ^{12}C is mixed to the stellar surface during the so-called "third dredge-up." After a number of dredge-up episodes, the star evolves into a carbon star ($C/O > 1$), now producing carbonaceous and SiC dust (e.g., Gail et al. [2009] and references therein). Based on their C-, N-, and Si-isotopic compositions, presolar SiC can also be divided into distinct populations (Hoppe and Ott et al., 1997). A detailed overview over the presolar SiC classification and the astrophysical background is given in Hoppe et al. (2010) and Zinner (2014).

CM chondrites are among the more primitive solar system materials and constitute the largest group of carbonaceous chondrites (Brearley and Jones 1998; Lauretta et al. 2000; Weisberg et al. 2006; Chizmadia and Brearley 2008). They have experienced varying degrees of aqueous alteration (McSween and Richardson 1977; Zolensky et al. 1993; Brearley and Jones 1998), representing mixtures of primary phases (e.g., chondrules, Ca-Al-rich inclusions, Fe,Ni metal,

anhydrous silicates, sulfides), and secondary phases like phyllosilicates and Fe-oxides, often intergrown on the micrometer to submicrometer scale (Lauretta et al. 2000; Zega and Buseck 2003; Chizmadia and Brearley 2008). This makes them valuable targets for the investigation of the effects of aqueous alteration on primitive components of the solar nebula. One characteristic feature of CM chondrites is the presence of fine-grained dust rims (FGRs) around chondrules (Fig. 1) and other similarly large constituents that are texturally distinct from the interchondrule matrix (Fuchs et al. 1973; Grossman et al. 1988; Metzler et al. 1992; Zolensky et al. 1993; Hanowski and Brearley 2000, 2001; Liffman and Toscano 2000; Hua et al. 2002; Vogel et al. 2003; Zega and Buseck 2003; Cuzzi 2004; Trigo-Rodriguez et al. 2006). Various different models of rim formation have been suggested, including parent-body scenarios like chondrule erosion or accretion in the regolith (Sears et al. 1993; Tomeoka and Tanimura 2000; Trigo-Rodriguez et al. 2006), but a nebular origin is now widely accepted (Metzler et al. 1992; Ciesla et al. 2003; Chizmadia and Brearley 2008; Hanna and Ketcham 2018). One fundamental obstacle in the discussion of these formation scenarios is the fact that different structures are designated as "fine-grained rims" or "fine-grained chondrule rims." The FGRs investigated in this study (Table 1) share certain properties with the FGRs studied in CO (Davidson [2009]; Haenecour et al. [2018]and references therein) and CR chondrites (e.g., Leitner et al. 2016), such as the presence of primitive components showing little signs of alteration, in close correlation (often at the submicrometer scale) with constituents that have experienced aqueous alteration. In contrast, the FGRs described by Tomeoka and Tanimura (2000) and Takayama and Tomeoka (2012) in the Tagish Lake carbonaceous chondrite and several CV (Vigarano-type) chondrites consisted primarily of phyllosilicates and had experienced severe aqueous alteration.

The presence of presolar grains, especially presolar silicates, in the CR and CO FGRs, and their different abundances in the FGRs and the respective interchondrule matrices of the studied meteorites clearly advocates for a nebular origin of these structures (Leitner et al. 2016; Haenecour et al. 2018). Neither chondrule erosion nor accretion in the regolith could account for the presence of stardust grains or the observed abundance variations. In a nebular setting, free-floating chondrules would accrete rims from fine-grained dust (which contains presolar grains), and then form planetesimals/meteorite parent bodies together with "rimless" chondrules, other larger constituents, and the remaining fine-grained dust fraction.

Presolar grains from CM chondrites, especially from the well-studied Murchison meteorite, have been the subject of investigations for the past three decades. The vast majority of these investigations have been conducted on grain separates, only suitable for the most refractory types of dust (SiC, graphite, aluminum-rich oxides, nanodiamonds; Bernatowicz et al. 1987; Lewis et al. 1987; Zinner et al. 1987, 2003; Amari et al. 1990; Nittler et al. 1993, 1995). Nagashima et al. (2005) reported four presolar O-rich grains, potentially silicates, detected in situ in Murchison with a modified ims-1270 ion probe. They calculated an abundance of ~3 ppm, but due to the low spatial resolution (500–1000 nm) in comparison to the 100–150 nm typically used for NanoSIMS ion imaging, this abundance is not comparable to NanoSIMS-derived results, and likely underestimates the true abundance, because smaller grains are likely to remain undetected. More recently, Liebig and Liu (2014) detected one presolar Al-oxide and three presolar SiC grains by NanoSIMS ion imaging in Murchison, but no presolar silicates were reported.

Here, we report the results of a comprehensive in situ study of oxygen-rich and SiC stardust in the fine-grained chondrule rims within the CM chondrites Banten, Jbilet Winselwan, Maribo, Murchison, Murray, and Yamato 791198, and the CM-related Sutter's Mill meteorite (Jenniskens et al. 2012; Zolensky et al. 2014). Preliminary results were reported as conference papers (Leitner et al. 2013, 2014, 2015). The presence of stardust grains in the FGRs would further support a nebular origin of the rims and be in line with the detection of presolar silicates and oxides in FGRs from CO (Ornans-type) chondrites (Davidson 2009; Haenecour et al. 2018), CR (Renazzo-type) chondrites, and the ungrouped minimally altered C2 Acfer 094 (Leitner et al. 2016). Investigation of the presolar grain inventory of fine-grained chondrule rims in CM chondrites will allow for further study of the effects of secondary processing on the nebular materials which provided the building blocks of the larger solar system bodies. Moreover, the CMs bear some spectral similarities to several classes of Main Belt asteroids (B, C, F, and G groups; Vilas and Gaffey 1989; Gaffey et al. 1993), therefore representing potential reference material for the investigation of future samples collected from such asteroid types.

SAMPLES AND EXPERIMENTAL

We studied thin sections of the CM chondrites Banten, Jbilet Winselwan, Maribo, Murchison (two separate sections), Murray, and Yamato (Y-) 791198, together with a thin section from Sutter's Mill (SM2-3)

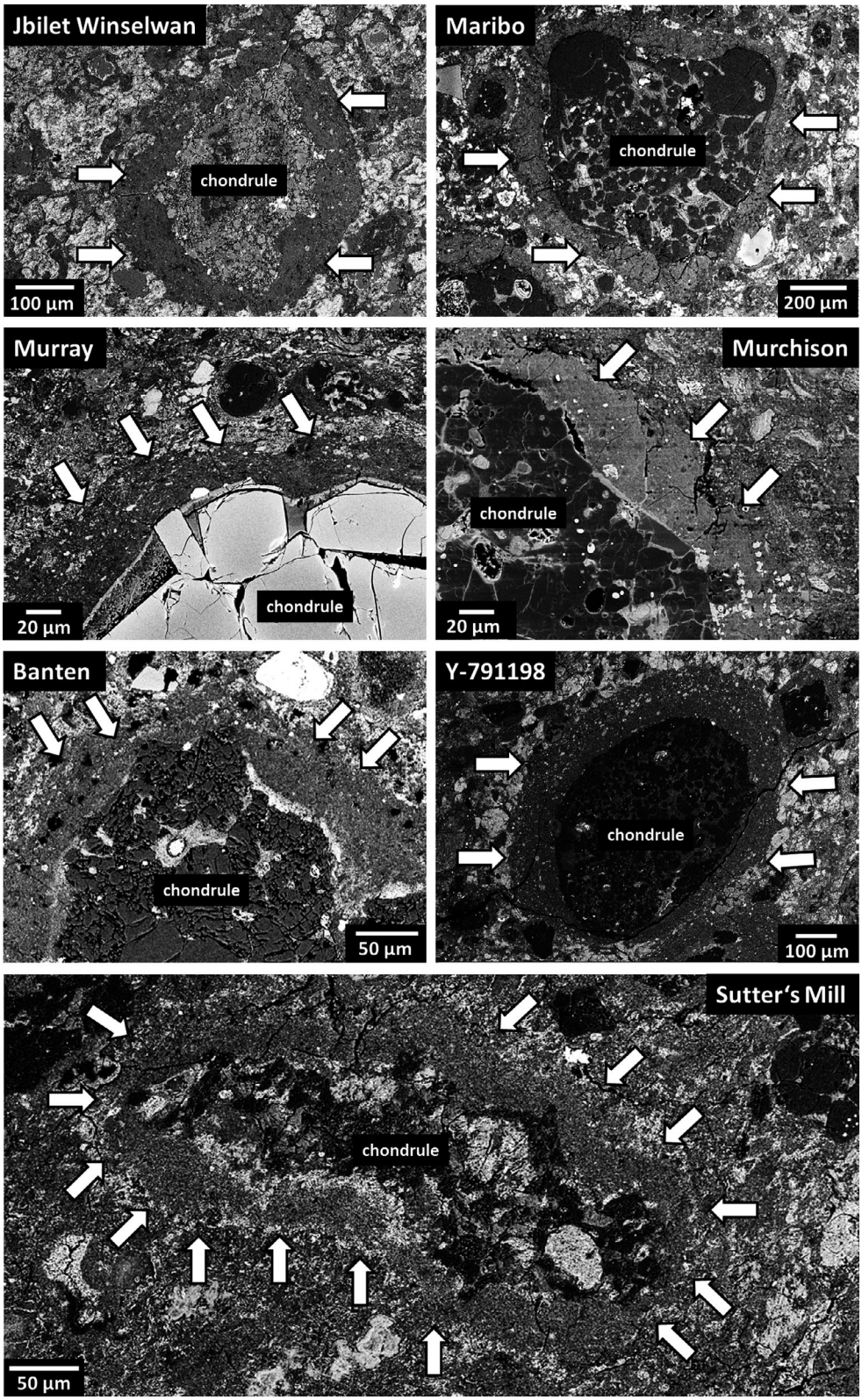

Fig. 1. Backscatter electron images showing examples of fine-grained chondrule rims from Jbilet Winselwan, Maribo, Murray, Murchison, Banten, Y-791198, and Sutter's Mill. The fine-grained rim material is highlighted in each panel by the white arrows.

Table 1. Samples investigated in this study.

Meteorite	Source	Sample no.	Scanned area (μm²)[a]	# of FGRs[b]	Petr. subtype[m]	Petr. subtype[n]	Petr. subtype[o]	Weath. grade
Murchison	MPIC	01[k]	1,650	1 [982]	2.5	2.5/1.6	1.5	W1-2,fall[m]
	MPIC	02	10,000	5 [713]				
Murray	MPIC	01[k]	11,800	3 [112]	2.4/2.5	2.5/1.6	1.5	W1-2,fall[m]
Maribo	IfP[c]	PL 15238	15,030	8 [282]	>2.7	N.d.[l]	N.d.	W0, fall[e]
Yamato-791198	NIPR[d]	61-7	16,250	5 [889]	2.4	2.5/1.5	1.6	W1[m]
Jbilet Winselwan	MPIC	01	20,250	7 [737]	N.d.	2.4[f]/1.5–1.8[g]	1.5[g]	W1[h]
Banten	MPIC	6017-2	10,900	5 [193]	N.d.	2.5/1.7	N.d.	Fall
Sutter's Mill (SM2-3)	IfP	PL 12040	10,130	7 [20]	2.0/2.1	N.d.	N.d.	W0, fall[i,j]
Total (without Sutter's Mill)			85,880	34				

[a]Area investigated by NanoSIMS ion imaging.
[b]Number of fine-grained rims searched for presolar grains; the total number of FGRs for each thin section is given in brackets.
[c]Institute for Planetology, Westfälische Wilhelms-Universität, Münster, Germany.
[d]National Institute for Polar Research, Japan.
[e]Haack et al. (2012).
[f]Calculated after Alexander et al. (2013) with bulk-$^{15}N/^{14}N$-data from King et al. (2019).
[g]King et al. (2019).
[h]Ruzicka et al. (2015).
[i]Ruzicka et al. (2014).
[j]Specimen SM2-3 was collected before rain (Jenniskens et al. 2012).
[k]Thin section produced from material supplied by Uli Ott (MPIC).
[l]n.d.: Not determined.
[m]Rubin et al. (2007); based on a set of mineralogic and textural properties (e.g., matrix silicate abundance, chondrule mesostasis, abundance and composition of tochilinite-cronstedite intergrowths).
[n]Alexander et al. (2013). Numbers before the slash: Determined from the bulk-N-isotopic compositions, largely comparable to the Rubin et al. (2007) classification; numbers after the slash: classification based on bulk water/OH H contents; compatible with the classification by Howard et al. (2015).
[o]Howard et al. (2015).

(Table 1). Petrological subtypes from three different classification schemes (Rubin et al. 2007; Alexander et al. 2013; Howard et al. 2015) are included in Table 1. Prior to the SIMS analyses, suitable target areas within fine-grained rims were identified and documented by scanning electron microscopy. The two main criteria for area selection were (1) absence/preferably low occurrence of larger ($d \gg 1$ μm) constituents in the areas, and (2) little/no indications of (extensive) aqueous alteration. We selected five FGRs (out of 193) from Banten, seven (out of 737) from Jbilet Winselwan, eight (out of 282) from Maribo, six (out of 1695) from Murchison, three (out of 112) from Murray, five (out of 889) from Y-791189, and seven rims out of 20 from Sutter's Mill (Table 1).

Scanning Electron Microscopy and SEM-EDS

Samples (Table 1) were characterized by backscatter electron (BSE) imaging and X-ray elemental mapping with an LEO 1530 field emission scanning electron microscope (FE-SEM) equipped with an Oxford X-max 80 silicon drift EDS detector at the Max Planck Institute for Chemistry (MPIC) in Mainz. For data acquisition, Oxford's Aztec software suite was utilized. Quantitative element data were acquired without external standards. The accuracy of the system was determined in a previous study (Leitner et al. 2018) by measuring a suite of standard minerals with known compositions.

Nanoscale Secondary Ion Mass Spectrometry (NanoSIMS)

Suitable FGRs were selected for O-isotopic analysis to search for presolar O-rich grains with the NanoSIMS 50 ion probe at the MPIC. Carbon and silicon isotopes were measured for SiC-candidates in Murray, Maribo, Jbilet Winselwan, Banten, and Sutter's Mill identified by ^{28}Si-hotspots (i.e., small high-intensity areas accompanied by low ^{16}O-intensities) during the O isotope measurements. The success rate for this approach depends on how much synthetic SiC has been deposited in the respective meteorite sections during sample preparation and polishing, but lies typically between 80% and 95%. However, it should be noted that this approach might introduce a bias to the sizes of detected grains, since SiC does not *always* display significantly enhanced ^{28}Si-intensities in comparison to the surrounding matrix silicates. This could lead to a

preferential detection of larger grains. The thin sections of Murchison and Y-791198 had to be recoated after initial NanoSIMS investigation, and the measurement fields containing the SiC-candidates could not be relocated.

Prior to O-isotopic analyses, fields of 14 × 14 μm² were sputtered with a high current primary beam (~20 pA) to remove the carbon coating on selected sample areas. All measurements were conducted in ion imaging mode, where a primary Cs^+ beam (100 nm diameter, ~1 pA) was rastered over 3 × 3 μm²- to 10 × 10 μm²-sized sample areas. Ion counting rates of $^{12}C^-$, $^{16}O^-$, and $^{28}Si^-$ were corrected for quasi-simultaneous arrivals with correction factors according to Slodzian et al. (2004) and Hillion et al. (2008). Corrections were applied individually for each grain or region of interest.

O-isotopic analyses were performed in "chained analysis" mode; that is, after defining a starting position, measurements are conducted automatically, with the sample stage moving in a predefined pattern. For data reduction and processing, in-house software developed at the MPIC ("Nano50Isotopes") was used.

Oxygen Isotopic Measurements

Secondary ion images of $^{16}O^-$, $^{17}O^-$, $^{18}O^-$, $^{28}Si^-$, and $^{27}Al^{16}O^-$ were acquired in multicollection mode to identify O-anomalous presolar signatures. Each measurement consisted of five image planes of 11 minutes integration time each over 10 × 10 μm² areas (256 × 256 pixels). Presolar O-rich grains were then identified by their anomalous O-isotopic compositions with respect to surrounding material. Simultaneous detection of $^{28}Si^-$ and $^{27}Al^{16}O^-$ allowed for a first-order distinction between silicates and Al-rich oxides (Fig. 2). The often-adopted 4σ-criterion has been found to be insufficient for the identification of presolar grains (Hoppe et al. 2015). Thus, we used the 5.3σ-criterion from the aforementioned study for the identification of presolar isotope anomalies, together with the requirement that the isotopic anomaly is present in at least three subsequent image planes. In the grain identification process, the 50% contour lines around identified anomalous grains (minima and maxima) were applied, and significance levels were calculated from the confidence limits for Poisson statistics of small numbers (Gehrels 1986). Generally, confidence limits should not be calculated simply from the square root of the detected counts when statistics of small numbers are involved. This is because the Poisson distribution is asymmetric for small mean number of counts. We will demonstrate this by the example of grain HR-E@1-11-1 from Hoppe et al. (2015). This grain has $\delta^{17}O = 785 \pm 173$ ‰, which gives a significance of 4.5 σ when statistics based on the square root of the counts is applied. The procedure of Gehrels (1986) takes the asymmetry of the Poisson distribution into account. The equations use two parameters (β, γ) which depend on the confidence limit (table 3 of Gehrels 1986). Both parameters are given up to confidence limits corresponding to 3.3 σ. As these two parameters vary only smoothly for confidence limits larger than 3 sigma, we expanded the Gehrels approach to confidence limits larger than 3.3 σ, using the β and γ values for 3.3 σ. Using the respective equations gives a significance of 5.4 σ for the ^{17}O anomaly of grain HR-E@1-11-1. We have verified this approach by numerically integrating the Poisson distribution (106 counts measured for ^{17}O, 59.4 counts calculated for ^{17}O for solar system composition), which gives a significance of 5.5 sigma. This demonstrates that the Gehrels approximation is quite robust, even for significances exceeding 3.3 σ. For larger number of counts, as in the present study, the difference between the significances calculated from the square root of the counts and Gehrels/numerical integration gets smaller. We note that all grains from the present study, except Y_2_16, have significances of more than 5.3 σ, even when using "square root" statistics. We chose to use the 5.3 sigma limit here instead of the usually used 4 sigma limit to be consistent with the work of Hoppe et al. (2015), even if the measurements presented here were done with different measurement conditions. Moreover, typical numbers of ^{17}O counts are not very different (median values of 110 in Hoppe et al. [2015] versus 180 in the work presented here), which results from the fact that image dimensions were a factor of 2 lower and integration times longer in Hoppe et al. (2015). If we would have used a 4 σ criterion here for presolar grain identification, only one additional grain would have been identified, that is, the selection of the σ-limit has no big impact on the discussion of our data.

The measured O-isotopic compositions of presolar silicates and oxides were normalized to O-rich material from the surrounding matrix, which was assumed to have solar system isotopic ratios (Table 2; the spread of O-isotopic compositions found in the vast majority of matter of unequivocally solar system origin is smaller than the typical measurement uncertainty of the NanoSIMS measurements reported here, so normalizing our grain data on a single isotope ratio assumed for the matrix is justified).

Not all presolar grain sizes reported here could be determined from SEM images; we had to rely on the secondary ion images instead. In these instances, the sizes are reported as "a × b" (in nm), with "a" and "b" being the major and minor axis of an elliptical approximation of the grain. To determine average grain sizes, we recalculated the grain diameters from the

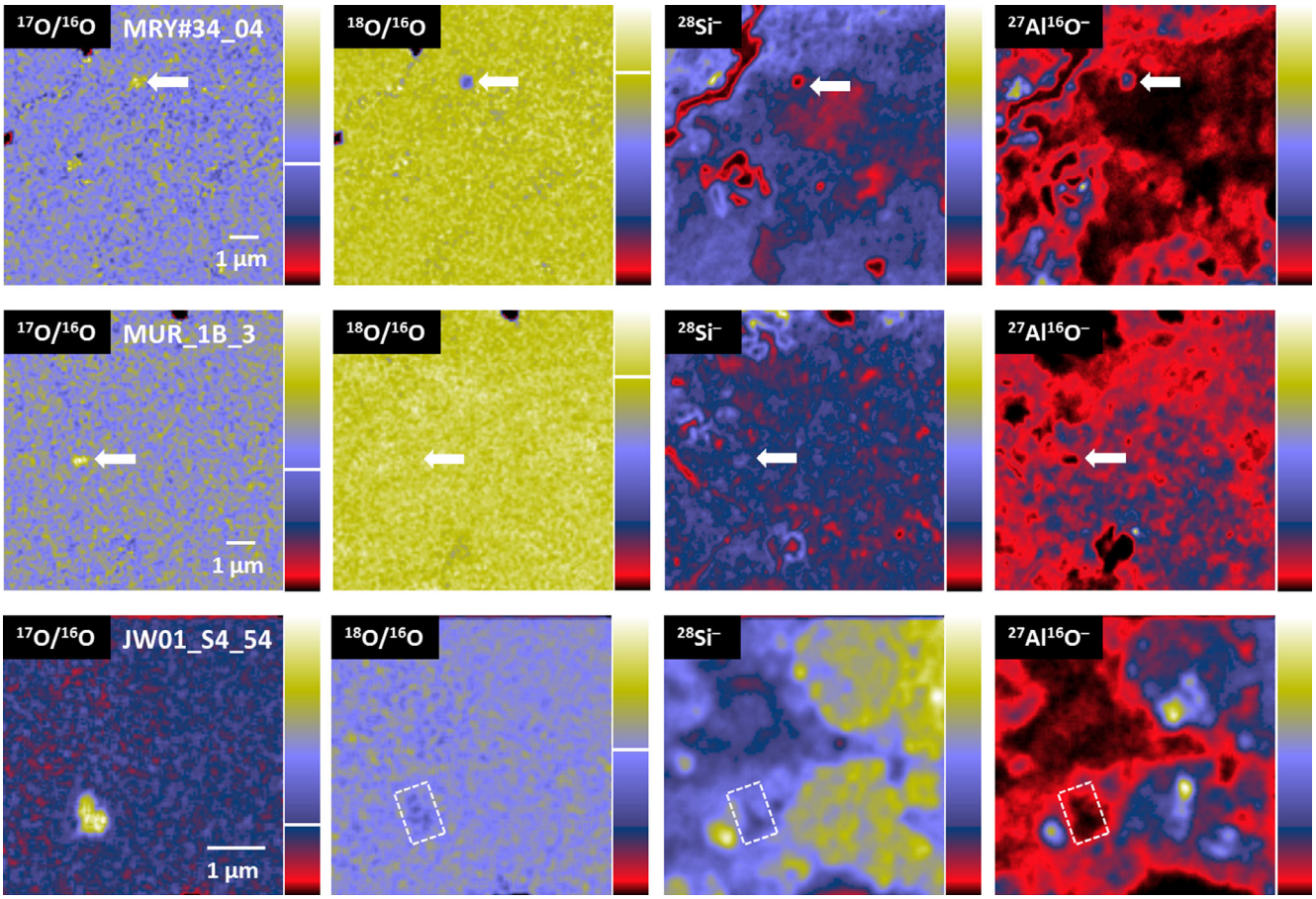

Fig. 2. Isotope ratio images of $^{17}O/^{16}O$ and $^{18}O/^{16}O$, together with secondary ion images of $^{28}Si^-$ and $^{27}Al^{16}O^-$ (from left to right) for oxide grain MRY#34_04 from Murray (top row), silicate grain MUR_1B_3 from Murchison (center row), and silicate grain JW01_S4A_54 from Jbilet Winselwan (bottom row). The positions of the presolar grains are marked by white arrows (top and center rows) and by a rectangular box (dashed white line, bottom row). Color scale bars are displayed for each image, ranging from black (no intensity) over red and blue to yellow and white (highest intensities). For the O-isotopic ratio images, the respective terrestrial values are marked by white lines in the color scale bars. Grain details are given in Table 2; Tables A1 and A2. (Color figure can be viewed at wileyonlinelibrary.com.)

respective grain areas by assuming a circular outline with the same area.

Carbon and Silicon Isotopic Measurements

Secondary ion signals of $^{12}C^-$, $^{13}C^-$, $^{28}Si^-$, $^{29}Si^-$, and $^{30}Si^-$ were detected simultaneously in multicollection mode. Five to ten image planes of 4 min integration time each were acquired over 3 × 3 µm²- to 4 × 4 µm²-sized areas (128 × 128 pixels). Carbon-isotopic ratios were normalized to those measured on a synthetic SiC-standard with a known composition of $\delta^{13}C_{PDB} = -29‰$, and the Si-isotopic ratios of each grain were normalized to the ratios of the whole ion image (assuming terrestrial isotopic composition for the surrounding matrix material), after confirming that no significant deviations between the isotopic composition of the standard and the respective sample areas existed. Silicon-isotopic anomalies are reported as δ-values, which give the deviation from a reference ratio in ‰:

$$\delta^{29,30}Si = [(^{29,30}Si/^{28}Si)_{sample}/(^{29,30}Si/^{28}Si)_{reference} - 1] \times 1000‰$$

Auger Electron Spectroscopy

Major element compositions of six presolar grains from Murchison, Murray, and Jbilet Winselwan were analyzed with the PHI 700 Auger Nanoprobe at Washington University in St. Louis, using established procedures for presolar silicate grains (Stadermann et al. 2009; Floss 2018). In brief, after surface sputter cleaning with a widely defocused 2 kV, 1 µA Ar^+ ion beam, Auger electron energy spectra were obtained with a 10 kV

Table 2. Presolar silicates and oxides identified in the CM chondrites analyzed in this study. "Gr." denotes the group of the respective grain, in accordance with the classification by Nittler et al. (1997, 2008). "Ph." gives the phase of the grain (sil.: silicate, Al-/Fe-ox.: Al-/Fe-oxide). Grain sizes were determined from SEM images unless noted otherwise. All errors are 1σ.

Meteorite	Grain	Size (nm)	$^{17}O/^{16}O$ ($\times10^{-4}$)	$^{18}O/^{16}O$ ($\times10^{-3}$)	Gr.	Ph.
Murchison	MUR#001_1B_1	280 × 375	5.96 ± 0.38	1.96 ± 0.07	1	Sil.[b]
Murchison	MUR#001_1B_3	280 × 530	5.73 ± 0.24	2.00 ± 0.04	1	Sil.[b,c]
Murchison	MUR_2_01_21	230 × 230	3.27 ± 0.30	2.43 ± 0.08	4	Sil.[b]
Y-791198	Y_2B_42	440 × 325[a]	5.16 ± 0.74	1.15 ± 0.11	1	Sil.[b]
Y-791198	Y_2_16	400 × 325[a]	5.11 ± 0.29	1.92 ± 0.06	1	Sil.[b]
Maribo	MAR-R_B_32	350 × 280[a]	14.78 ± 1.28	1.72 ± 0.14	1	Al-ox.[b]
Maribo	MAR-R_C2_34	245 × 245[a]	5.83 ± 0.58	2.85 ± 0.13	4	Al-ox.[b]
Maribo	MAR-R_A_29	185 × 300[a]	4.94 ± 0.41	1.50 ± 0.07	1	Sil.[b]
Murray	MRY#20_07	210 × 270	9.67 ± 0.99	2.19 ± 0.15	1	Sil.[b,c]
Murray	MRY#34_04	555 × 435	6.15 ± 0.55	0.89 ± 0.11	2	Al-ox.[b,c]
Murray	MRY#34_19	550 × 250	5.82 ± 0.26	2.01 ± 0.05	1	Al-ox.[b,c]
Murray	MRY#20_04	170 × 220	5.75 ± 0.35	1.93 ± 0.08	1	Al-ox.
Jbilet Winselwan	JW01_02B_02	535 × 340	4.57 ± 0.34	2.80 ± 0.07	4	Fe-ox.[c,d]
Jbilet Winselwan	JW01_S4A_28	265 × 120	6.97 ± 0.52	1.98 ± 0.09	1	Sil.[b,c]
Jbilet Winselwan	JW01_S4A_54	490 × 735	12.26 ± 0.03	1.70 ± 0.04	1	Sil.[b,d]
Solar system			3.81	2.01		

[a]Grain size determined from NanoSIMS secondary ion images.
[b]Phase determined from NanoSIMS ion images.
[c]Phase determined by AES.
[d]Phase determined by SEM-EDS.

primary electron beam (0.25 nA), which was rastered over the grains of interest. The lateral resolution was 20–25 nm, with an information depth of a few nm. Twenty spectral scans over a small area of a given grain are combined to obtain a single Auger spectrum, which is subjected to a 7-point Savitsky–Golay smoothing and differentiation routine prior to peak identification and quantification. Sensitivity factors for O, Si, Fe, Mg, Ca, and Al were determined from olivine and pyroxene standards of various compositions (Stadermann et al. 2009). Errors are based on the 1σ-uncertainties of the sensitivity factors (O: 3.6%; Si: 11%; Fe: 11.2%; Mg: 9.4%; Ca: 10.8%; Al: 24.9%) and should be considered lower limits, since they do not include corrections for background noise, or take into account other factors potentially affecting the quality of a spectrum (e.g., sample charging, residual surface contamination). Detection limits are element dependent, but are typically in the range of a few atom percent. In addition, elemental distribution maps (3 × 3 μm² field of view, 256 × 256 pixels) of two of the grains (JW01_02B_02 and MRY_34_19) and the surrounding meteorite matrix were acquired at 10 keV and 10 nA, with 5–30 scans (depending on the element mapped).

Focused Ion Beam (FIB) Preparation and Transmission Electron Microscopy (TEM)

One electron-transparent lamella was prepared successfully from presolar silicate grain JW01_SA4_54 from Jbilet Winselwan with the focused ion beam (FIB) technique (Wirth 2004; Zega et al. 2007), using an FEI Quanta 3D FEG at the Institute of Geosciences, Friedrich Schiller University (IGW-FSU), Jena. Sample preparation followed standard protocols (e.g., Harries and Zolensky 2016). Subsequent field-emission TEM analyses were performed with an FEI Tecnai G^2 FEG at IGW-FSU, and with a Zeiss Libra 200FE equipped with an in-column Omega energy filter at the Institute for Mineralogy, University of Münster. Both TEMs were operated at 200 kV. We used conventional brightfield (BF) TEM imaging for diffraction contrast imaging, and the "high angle annular darkfield" (HAADF) detector in scanning TEM mode for Z contrast imaging. Energy-dispersive X-ray spectra were recorded in conventional TEM mode using a defocused beam with integration times of several tens of seconds to obtain sufficient counting statistics using an Oxford X-Max^n 80T SDD-EDS detector.

RESULTS

Presolar O-Anomalous Grains

A total area of 85,880 μm² in FGRs from six CM chondrites (Table 1) has been searched for O-anomalous presolar grains (silicates and oxides), together with 10,130 μm² in Sutter's Mill. We identified 15 O-anomalous grains (nine silicates, six oxides) in the CMs (Table 2; Figs. 3 and 4), with sizes ranging from

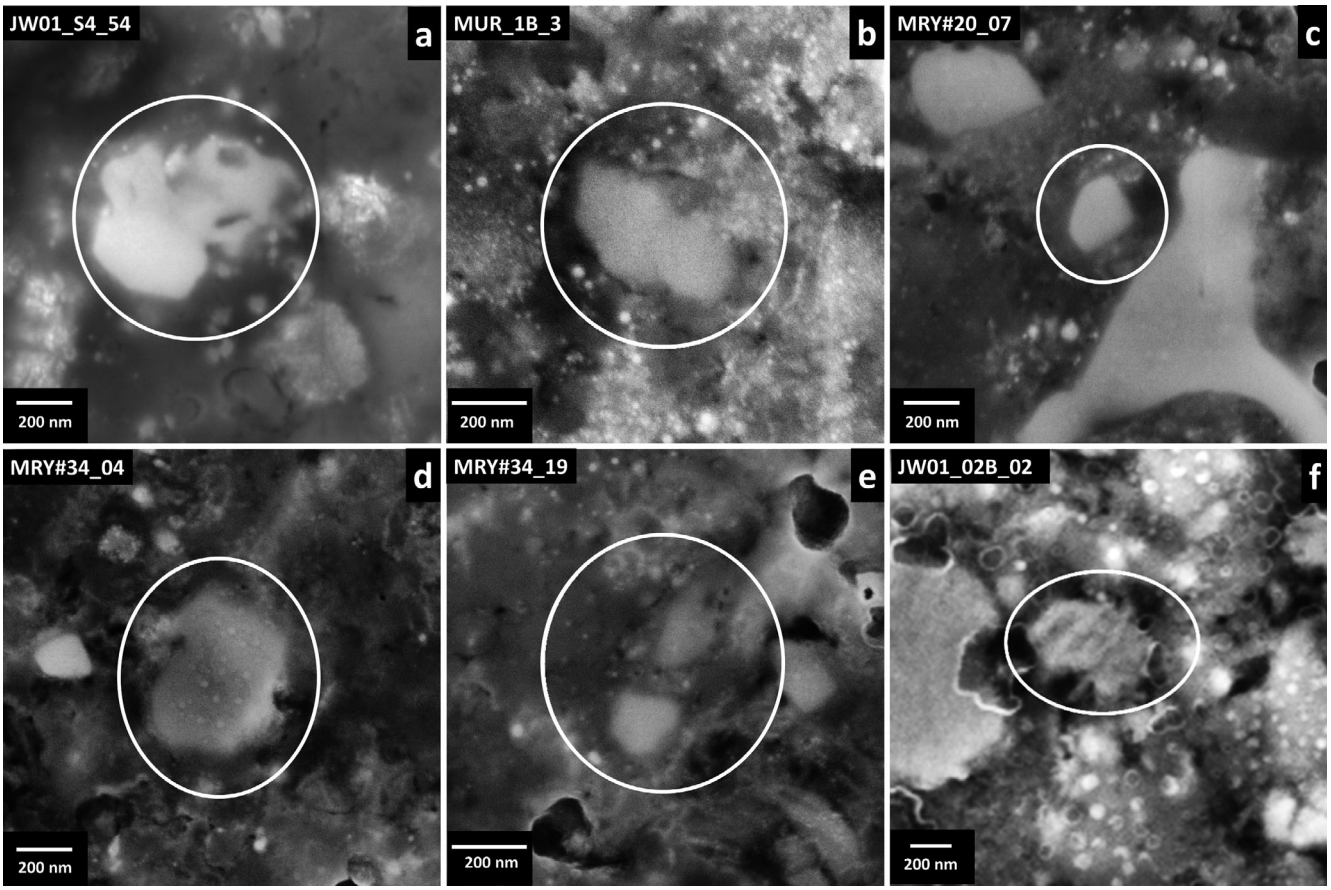

Fig. 3. Scanning electron microscopy (SEM) micrographs showing examples of the presolar O-rich grains investigated in this study (marked by white circles). a) JW01_S4A_54 from Jbilet Winselwan (Mg-Ca-silicate, determined by SEM-EDS and transmission electron microscopy), b) MUR_1B_3 from Murchison (Fe-rich silicate), c) MRY#20_07 from Murray (Mg-silicate, determined by auger electron spectroscopy [AES]), d) MRY#34_04 from Murray (Al-oxide with spinel-like composition, determined by SEM-EDS and AES), e) MRY#34_19 from Murray (Al-oxide with spinel-like composition, determined by SEM-EDS and AES), f) JW01_02B_02 from Jbilet Winselwan (Fe-oxide, determined by SEM-EDS and AES).

180 to 600 nm for the silicates and 190–490 nm for the oxides; no O-anomalous grains were found in the areas analyzed in Banten or in Sutter's Mill. Grain diameters were determined either from high-resolution SEM images, or, if not available, estimated from secondary ion images (see Table 2).

Murchison and Y-791198 contained three and two silicates, respectively. Three presolar grains were found in each of Maribo and Jbilet Winselwan (two Al-oxides and one silicate, and two silicates and one Fe-oxide, respectively), and four in Murray (one silicate, three Al-rich oxides). Twelve grains belong to Group 1, with $^{17}O/^{16}O$ ratios ranging from $4.88 \pm 0.21 \times 10^{-4}$ to $14.78 \pm 1.28 \times 10^{-4}$, and $^{18}O/^{16}O$ ratios between $1.15 \pm 0.11 \times 10^{-3}$ and $2.30 \pm 0.12 \times 10^{-3}$. One Al-oxide from Murray falls into Group 2, with $^{17}O/^{16}O = 6.15 \pm 0.55 \times 10^{-4}$ and $^{18}O/^{16}O = 0.89 \pm 0.11 \times 10^{-3}$. Finally, three grains are from Group 4, with enhanced $^{18}O/^{16}O$ ratios compared to the terrestrial value, ranging from $2.43 \pm 0.08 \times 10^{-3}$ to $2.85 \pm 0.13 \times 10^{-3}$, and $^{17}O/^{16}O$ varying between $3.27 \pm 0.30 \times 10^{-4}$ and $5.83 \pm 0.58 \times 10^{-4}$.

Presolar Silicon Carbide Grains

We identified 21 presolar SiC grains in Murray, Maribo, Jbilet Winselwan, Banten, and Sutter's Mill (Fig. 5). Eighteen grains are mainstream (MS) grains, with $^{12}C/^{13}C$ ratios ranging from 43.1 ± 0.6 to 90.2 ± 1.4, and Si-isotopic compositions of $\delta^{29}Si = -6 \pm 19$ ‰ to 111 ± 21 ‰ and $\delta^{30}Si = -12 \pm 12$ ‰ to 133 ± 58 ‰. Three grains are of type AB, with $6.8 \pm 0.5 \leq {}^{12}C/^{13}C \leq 7.7 \pm 0.1$, -1 ± 40 ‰ $\leq \delta^{29}Si \leq 54 \pm 13$ ‰, and -49 ± 48 ‰ $\leq \delta^{30}Si \leq 42 \pm 16$ ‰.

Presolar Grain Abundances

The identified presolar silicate and oxide grains represent an average O-anomalous grain abundance of

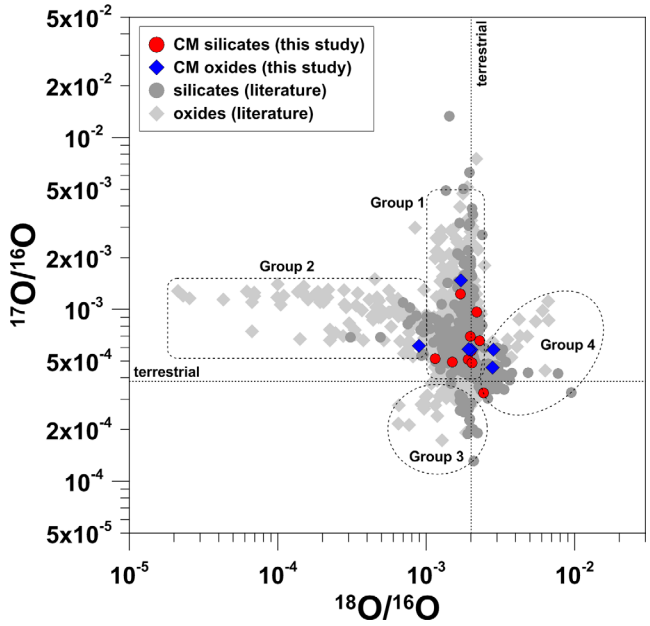

Fig. 4. Oxygen three-isotope plot showing the isotopic ratios of presolar silicates (red circles) and oxides (blue diamonds) found in five of the six CM chondrites of this study (no grains were found in Banten). The four main groups according to Nittler et al. (1997, 2008) are marked by the dashed black lines. Literature data of presolar silicates and oxides (gray symbols, "literature"; Nittler et al. 1993, 1994, 1997, 1998, 2008; Huss et al. 1994; Hutcheon et al. 1994; Strebel et al. 1997; Choi et al. 1998, 1999; Nittler and Alexander 1999, 2003; Krestina et al. 2002; Messenger et al. 2003, 2005; Nguyen et al. 2003, 2007, 2010; Zinner et al. 2003, 2005; Mostefaoui and Hoppe 2004; Nagashima et al. 2004; Nguyen and Zinner 2004; Floss et al. 2006, 2008; Marhas et al. 2006; Stadermann et al. 2006; Bland et al. 2007; Vollmer et al. 2007, 2008, 2009; Yada et al. 2008; Busemann et al. 2009; Floss and Stadermann 2009a, 2012; Bose et al. 2010a, 2010b; Gyngard et al. 2010; Keller and Messenger 2011). Errors are 1σ. The solar system average ratios are indicated by the dashed lines. (Color figure can be viewed at wileyonlinelibrary.com.)

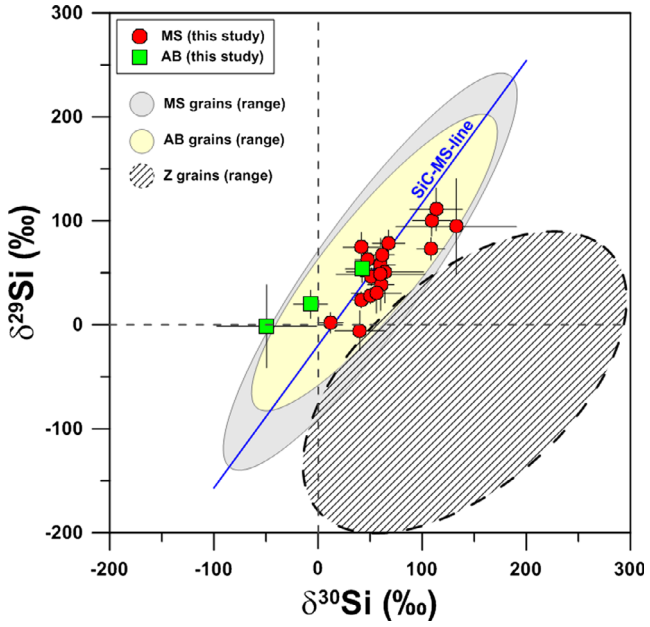

Fig. 5. Three-isotope plot for silicon showing data for the 21 SiC grains discovered in this study. The compositional range observed for MS, AB, and Z grains is marked by the oval shapes. Solar system composition is denoted by the dashed lines. All displayed errors are 1σ. The blue line denotes the SiC mainstream line (Zinner et al. 2006). (Color figure can be viewed at wileyonlinelibrary.com.)

18 (+5/–5) ppm for the six CM chondrites studied here (excluding Sutter's Mill), with a silicate abundance of 11 (+5/–4) ppm, and an oxide abundance of 8 (+4/–3) ppm (the sum of the silicate and oxide abundances differs from the O-anomalous abundance due to rounding issues). The O-anomalous grain abundances of the individual meteorites range from 11 (+11/–6) ppm for Maribo to 44 (+30/–19) ppm for Murray, and upper limits of 15 ppm for Banten and Sutter's Mill (Table 3).

The average SiC abundance is 42 ± 10 ppm, with individual abundances between 21 (+20/–11) ppm and 64 (+51/–31) ppm. As we pointed out earlier, no SiC abundances could be determined for Murchison and Y-791198. The confidence level of all errors is 1σ (unless stated otherwise) and is based on Poisson statistics. Asymmetrical errors were determined by the method for small numbers described by Gehrels (1986).

Elemental Compositions of Presolar O-Anomalous Grains

Major element compositions of six presolar grains from Murchison, Murray, and Jbilet Winselwan were obtained by auger electron spectroscopy (AES). Quantitative data could be determined successfully for five of these grains (Table A1 in Appendix), while JW01_02B_02 could only be qualitatively identified as Fe-oxide, with, potentially, a small Mg-content (Fig. 6a). Grain MUR_1B_3 turned out to be compositionally heterogeneous; the left part of the grain in Fig. 3b is Si-rich, with (Mg+Fe)/Si = 0.5, and Mg-free (with no Mg above detection limits), while the right part has an Fe-rich olivine-like composition, with Mg# = 28 (with Mg# = Mg/[Mg+Fe] × 100). Silicate grain JW01_S4A_28 is also Fe-rich (Mg# = 29), but Si-poor, with (Mg+Fe)/Si = 2.5 (Table A1 in Appendix). Silicate MRY_20_07 is of the "intermediate" type (Stadermann et al. 2009), showing an (Mg+Fe)/Si ratio of 1.5 ± 0.2, and Mg-rich (with no Fe above detection limits). We also measured two Al-oxide grains, MRY_34_04 and MRY_34_19 (Fig. 6b), and found them to have spinel-like compositions (Table A1 in the

Table 3. Abundances of presolar silicate, oxide, and SiC grains (given in ppm) for the individual meteorites studied here. Errors are 1σ, and were calculated according to Gehrels (1986). In the last column, the numbers of grains of each type found in the respective meteorites are given.

Meteorite	Grain type	Abd. (ppm)	Error (+)	Error (–)	No. of grains
Murchison	O-rich	21	20	11	3
	Silicates	21	20	11	3
	Oxides	<14[b]			0
	SiC	n.m.[a]			
Yamato 791198	O-rich	13	17	9	2
	Silicates	13	17	9	2
	Oxides	<10[b]			0
	SiC	N.m.[a]			
Maribo	O-rich	11	11	6	3
	Silicates	3	7	2	1
	Oxides	8	11	5	2
	SiC	48	24	17	8
Murray	O-rich	39	31	19	4
	Silicates	11	26	9	1
	Oxides	28	27	15	3
	SiC	37	29	18	4
Jbilet Winselwan	O-rich	25	24	13	3
	Silicates	15	20	10	2
	Oxides	9	22	18	1
	SiC	64	51	31	4
Banten	O-rich	<15[b]			0
	Silicates	<15[b]			0
	Oxides	<15[b]			0
	SiC	21	20	11	3
Sutter's Mill	O-rich	<15[b]			0
	Silicates	<15[b]			0
	Oxides	<15[b]			0
	SiC	25	33	16	2

[a]n.m.—not measured (see text for details).
[b]Upper limits; estimate based on the area calculated for a 250 nm-sized grain, with the upper 1σ-error added.

Appendix), with Al/Mg ratios of 3.1 ± 0.9 and 2.6 ± 0.7, respectively.

Transmission Electron Microscopy and SEM-EDS Analysis of JW01_S4A_54

The investigation of the relatively large (490 nm × 735 nm) silicate grain JW01_S4A_54 by AES was hampered by sample charging effects, but, due to its size, quantitative SEM-EDS was successful (spot analysis, lateral resolution ~400 nm at 5 kV; information depth ~300 nm). To monitor contributions from surrounding matrix material, we also obtained spectral data from four locations (about ~0.5–1 μm distance) surrounding the presolar grain. The results are summarized in Table A2 in the Appendix and show that no Ca is present in the neighborhood of JW01_S4A_54. The grain is an Mg-Ca-bearing silicate, with a diopside-like composition (Table A2 in the Appendix). The grain was subsequently prepared for TEM-analysis. Unfortunately, after some preliminary investigations, the TEM lamella was contaminated during handling, so no further structural data could be obtained. However, selected area electron diffraction (SAED) patterns indicate it to be crystalline. The observed lattice plane d-spacing of 0.548 nm is consistent with Mg-rich melilite (d_{110} = 0.553 nm in endmember åkermanite; Swainson et al. 1992) and rules out diopside as the main phase. A weaker reflection at d = 0.289 nm may belong to diopside, but this assignment is ambiguous. TEM-EDS spectra obtained before contamination qualitatively verify the SEM-EDS result, but were taken with a strongly defocused beam such that contributions from neighboring Fe-Mg silicates hamper the assessment of stoichiometry (Fig. 7a, approximate location from where the spectrum was obtained denoted by the yellow arrow). This is illustrated by the occurrence of Al, S, and Fe in the TEM-EDS spectrum, as well as by the presence of Cu from the copper grid.

DISCUSSION

Isotopic Signatures of Presolar Silicate and Oxide Grains

Most of the presolar silicates and oxides studied here (~75%) belong to Group 1 (Fig. 4), originating most likely from low-mass (~1.2–2.2 $M_\odot$) RGB/AGB stars (Nittler 2009; Palmerini et al. 2011). Their O isotope signatures are well explained by the "first dredge-up" (FDU) process, occurring when the star turns into a red giant star (Lattanzio and Boothroyd 1997; Boothroyd and Sackmann 1999). The star's surface composition is modified by the admixing of the products of partial H-burning, and its $^{17}O/^{16}O$ ratio is greatly enhanced (El Eid 1994; Boothroyd and Sackmann 1999). The stellar $^{18}O/^{16}O$ ratio is only marginally affected by the FDU, thus mainly representing the initial composition of the stellar envelope. However, recent Mg-isotope investigations found that a fraction (~10–15%) of the Group 1 grains originates from stellar sites undergoing explosive hydrogen-burning, most likely CCSN with H-ingestion (Leitner and Hoppe 2019), or super-AGB stars (M = 8–10 $M_\odot$), potentially ending their lives as so-called electron-capture supernovae (Nittler 2019; Verdier-Paoletti et al. 2019b). Thus, without Mg-isotopic data, there remains some uncertainty for the stellar sources of the Group 1 grains reported here. We compared the oxygen isotopic data of the grains from this study with presolar oxide grain data and the masses and initial

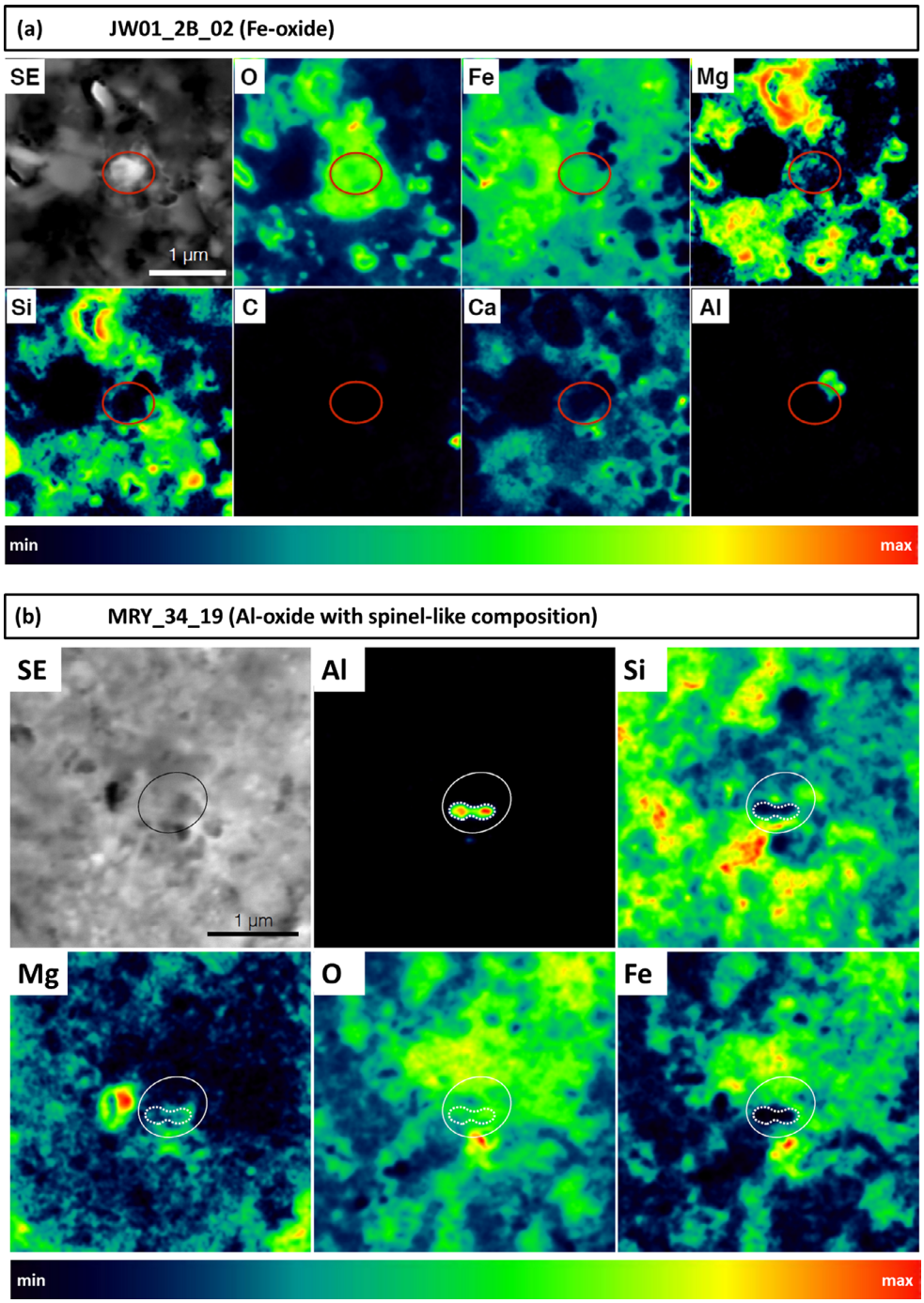

Fig. 6. Secondary electron images and false color element maps determined by auger electron spectroscopy for (a) the presolar Fe-oxide JW01_02B_02 and (b) the presolar Al-oxide grain MRY_34_19. In each image, the respective presolar grain is marked. The color bar represents a linear scale from black (zero intensity) to red (maximum intensity). (Color figure can be viewed at wileyonlinelibrary.com.)

$^{18}O/^{16}O$-ratios of their respective host stars relative to the solar value reported by Nittler et al. (2008). Eleven of the grains originate from stellar sources with masses in the range of 1.2–1.8 $M_{\odot}$, and metallicities ranging from about 0.9× to 1.5× the solar value. The last Group 1 grain (Y_2B_42) displays a $^{18}O/^{16}O$ ratio of $(1.15 \pm 0.11) \times 10^{-3}$, near the upper ratio limit for the Group 2 grains. This might be indicative of CBP in its parent star, which has been assumed for Group 1 grains with $^{18}O/^{16}O$ ratios below 1.5×10^{-3} (Nittler et al.

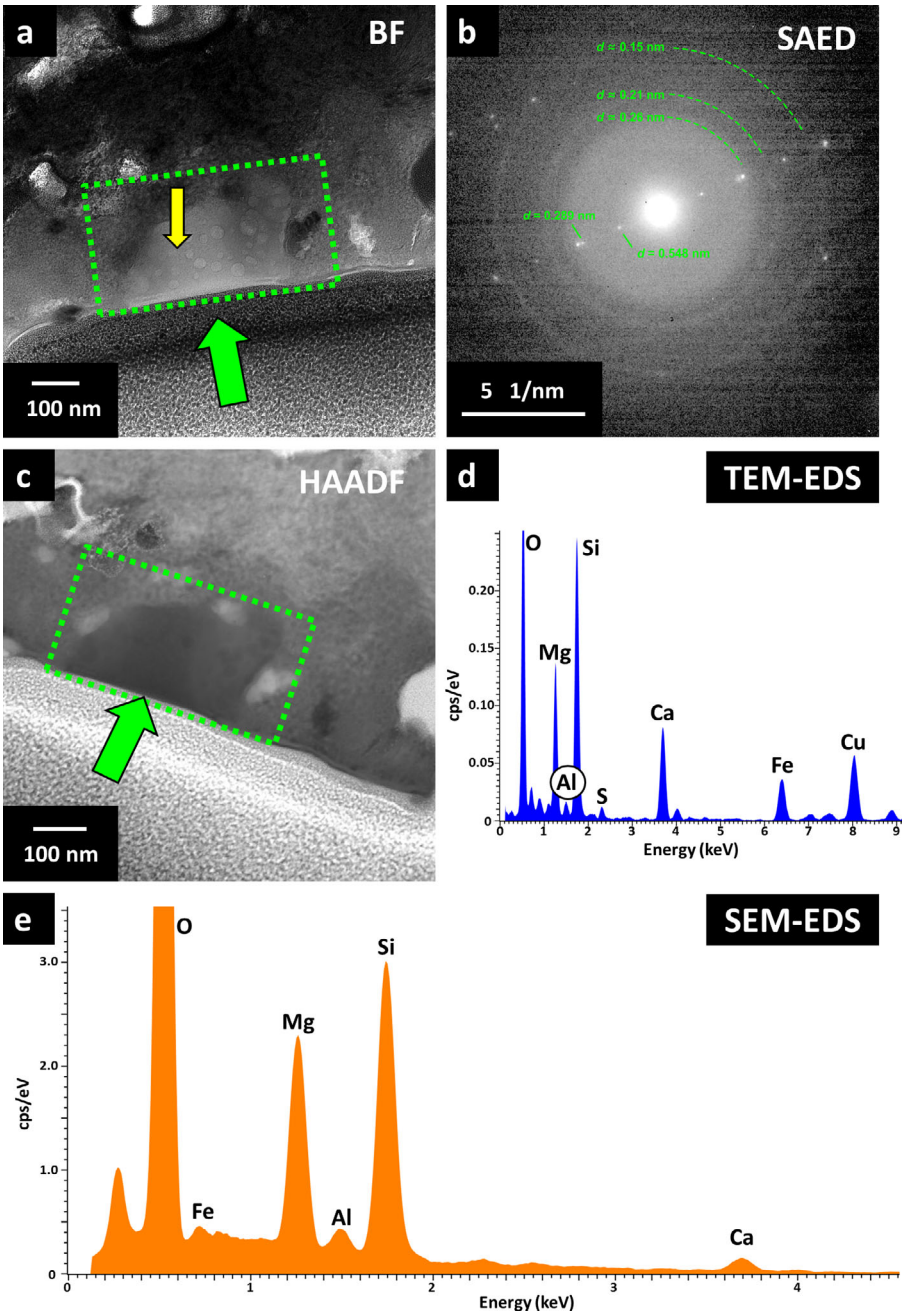

Fig. 7. Results from the transmission electron microscopy (TEM) investigation of silicate grain JW01_S4A_54 from Jbilet Winselwan. a) Brightfield (BF-)TEM image. The grain position is marked by the green arrow and the dotted rectangle; the yellow arrow denotes the approximate beam position of the TEM-EDS and selected area electron diffraction (SAED) analysis. Bubble-like features are due to beam damage sustained by TEM-EDS analysis. b) Log-scaled, low-dose SAED pattern of JW01_S4A_54 taken before EDS analysis, showing it to be crystalline and not amorphous. The array of reflections corresponds to a lattice plane d-spacing of 0.548 nm, consistent with (110) of Mg-rich, åkermanitic melilite. The d-spacing of 0.289 nm may correspond to Mg-rich silicate, potentially including diopside, in the area sample by the SAED aperture. Diffuse rings (d ≈ 0.15–0.26 nm) are from surrounding troilite- and magnetite-bearing material typically observed in the phyllosilicate-rich portions of Jbilet Winselwan (Harries, personal communication). c) STEM-HAADF image. The grain position is marked by the arrow and the dotted rectangle. d) TEM-EDS spectrum obtained from the grain, clearly showing the presence of Mg, Ca, and Al in the silicate. The Cu-signal stems from the copper grid on which the lamella was mounted. The presence of S indicates a contribution from surrounding matrix material. e) Scanning electron microscopy spectrum obtained with low acceleration voltage (5 kV) from the presolar grain. (Color figure can be viewed at wileyonlinelibrary.com.)

2008). A low metallicity effect, however, cannot be excluded. Nittler et al. (2008) stated that about one-third of the Group 1 oxides analyzed for Mg-isotopes showed no evidence for the presence of ^{26}Al, which would have been diagnostic for the occurrence of CBP. The observation that these ^{26}Al-free grains have $^{18}O/^{16}O$ ratios over the full range observed for Group 1 was then interpreted as evidence that the stellar parents of these grains did not experience additional mixing processes. Their $^{18}O/^{16}O$ ratios could rather be due to the lower-than-solar metallicities of the respective parent stars. In such a scenario, the depletion of ^{18}O relative to ^{16}O during the red giant phase is more pronounced, leading to lower $^{18}O/^{16}O$ ratios than for stars of solar metallicity. If we assume a low-metallicity-origin, the parent star of Y_2B_42 would have had a mass of M~1.3 $M_\odot$ and an initial $^{18}O/^{16}O$ ratio of ~0.7 times the solar ratio, according to Nittler et al. (2008). However, the destruction of ^{18}O begins already at temperatures below the activation temperature for effective ^{26}Al production (e.g., Nollett et al. 2003). Therefore, some of these grains may well represent stars with solar metallicity that experienced CBP, but did not synthesize significant amounts of ^{26}Al at the time of O-rich dust formation. One Group 2 spinel-like grain, MRY#34_04, is severely depleted in ^{18}O ($^{18}O/^{16}O = 0.89 \pm 0.11 \times 10^{-3}$), coming either from a 1.2–1.8 $M_\odot$ AGB star that experienced CBP, or from an intermediate-mass (4–8 $M_\odot$) AGB star with HBB (e.g., Lugaro et al. 2017).

The three Group 4 grains represent ~19% of the grain inventory. This number is higher than the 10% typically observed for >200 nm-sized presolar O-rich grains in primitive chondrites (Floss and Haenecour 2016), but the significance of this difference is unclear due to the very limited statistics. The grains display moderately enhanced $^{18}O/^{16}O$ ratios, while the $^{17}O/^{16}O$ scatter around the solar system value, being consistent with an origin in a 15 $M_\odot$ CCSN, with contributions from the Si/S (~0.05%), O/Ne (~0.15%), O/C (~1.9%), He/C (~1.1%), He/N (~4.8%), and H (~92.0%) zones (Rauscher et al. 2002; Vollmer et al. 2008; Nguyen and Messenger 2014).

Silicon Carbide Grains

Eighteen out of 21 SiC grains (~86%) found in this study show isotopic characteristics compatible with the observations from other meteoritic sample sets for MS SiC, supporting an origin in 1.5–3 $M_\odot$ AGB stars with ~solar metallicity (Lodders 2003; Zinner et al. 2006) (Table A3 in Appendix, Fig. 5). Three grains (~14%) are of type AB. Their origins are still under debate; possible sources include J-type carbon stars as well as born-again AGB stars, and an origin in CCSN e with explosive H-burning has been suggested (Amari et al. 2001; Fujiya et al. 2013; Liu et al. 2017a, 2017b; Nguyen et al. 2018; Schmidt et al. 2018).

Elemental Composition of Silicate and Oxide Stardust

The elemental compositions of presolar grains, especially silicates, can be used to gain insights into aqueous or thermal alteration affecting not only the grains themselves but (potentially) also the host meteorite. The three presolar silicates studied by AES and grain JW01_S4A_54 investigated by SEM-EDS and TEM represent, of course, too small a number to draw general conclusions about potential trends in grain compositions. Nevertheless, due to the relatively small number of presolar silicates and oxides studied by TEM compared to the number of grains identified by secondary ion mass spectrometry (<100 versus >1,500), any TEM data are a valuable addition to the existing data set. It should be noted that, despite the obvious aqueously altered state of the CMs, we still observed the full range of Mg-contents typical of presolar silicates from other chondrites, from Mg# = 0 to 100. The (Mg+Fe)/Si ratios also span the full compositional range observed for presolar silicates, from "Si-rich" (left part of MUR#001_1B_3; Fig. 3b), via "intermediate" (MRY_20_07), to "olivine-like" (right part of MUR#001_1B_3; Fig. 3b) and "Si-poor" (JW01_S4A_28). Presolar silicates in other primitive chondrites show the same range of compositions (Floss and Stadermann 2009a, 2012; Vollmer et al. 2009; Bose et al. 2010a, 2012; Nguyen et al. 2010; Zhao et al. 2013; Haenecour et al. 2018).

Grain JW01_S4A_54 is a Mg-Ca-bearing silicate. TEM investigation showed its structure to be compatible with åkermanite (Mg-rich melilite, $Ca_2Mg[Si_2O_7]$; Fig. 7b). In contrast, the previous SEM-EDS analysis indicated a diopside-like composition ($MgCaSi_2O_6$; Table A2 in the Appendix); that is, the Ca content is smaller than expected for near-endmember åkermanite. This conundrum can be resolved with the following considerations: We have to take into account that the excitation volume of the SEM-EDS measurement, even though conducted with 5 kV acceleration voltage, reaches deeper into the sample than the presolar grain (Fig. 7a and 7c). Let us now assume that the underlying matrix is virtually free of Ca (as is the fine-grained material *surrounding* the presolar grain, Table A2 in the Appendix). In this case, the measured grain composition would be diluted by Mg and Si from outside the grain, and the measured Ca-concentration would be lower than the true Ca content of JW01_S4A_54. Therefore, the *undiluted* composition

of the grain could indeed be compatible with åkermanite. The diffraction pattern (Fig. 7b) appears to indicate the presence of diopside besides the more pronounced åkermanite-pattern. In addition, the SEM image (Fig. 3a) shows a slight variation of contrast over the grain: the lower left portion of the grain appears to be somewhat brighter than the rest. This could indicate a compositional and/or structural difference; thus, JW01_S4A_54 could indeed be a composite grain, consisting of an intergrowth of åkermanite and diopside. Melilite and spinel are the first Mg-bearing phases condensing from a cooling gas in the typical pressure range for circumstellar outflows ($p \sim 10^{-10}$ bar to 10^{-6} bar) at temperatures of 1452 K and 1397 K, respectively. They are followed by anorthite ($CaAl_2Si_2O_8$, 1387 K), forsterite (Mg_2SiO_4, 1354 K), and diopside ($CaMgSi_2O_6$, 1347 K; Gail and Sedlmayr 1998, 1999; Lodders 2003). If we consider now total pressures and dust/gas-ratios in the typical range for circumstellar envelopes (e.g., $p^{tot} \sim 10^{-6}$ to 10^{-8} bar; Jeong et al. 2003), and dust/gas = 4×10^{-3} to 9×10^{-2} (by mass; Gobrecht et al. 2015), diopside condenses in fact at higher temperatures than forsterite. And if we further assume that the entire Al was already bound in other earlier formed minerals, condensation of diopside around an åkermanite core becomes feasible.

The two spinel-like grains from Murray both show Al/Mg ratios slightly higher than stoichiometric (3.1 ± 0.9 and 2.6 ± 0.7, calculated from Table A1 in the Appendix). Given the comparably large errors, this observation is not significant, although there are some indications that the presolar spinels from Murray might indeed have elevated Al/Mg ratios (Zinner et al. 2005; Gyngard et al. 2010). High temperature processing has been suggested (Gyngard et al. 2010), similar to observations made for spinels in Ca-Al-rich inclusions (Simon et al. 1994). However, for the Murray spinels studied by Gyngard et al. (2010), it could not be fully ruled out that the higher Al/Mg ratios resulted from artifacts of the SIMS measurements (caused by the differing ionization efficiencies of Mg and Al in combination with measurement times not long enough to allow for full equilibration of the ion signals, e.g., Lin et al. 2010).

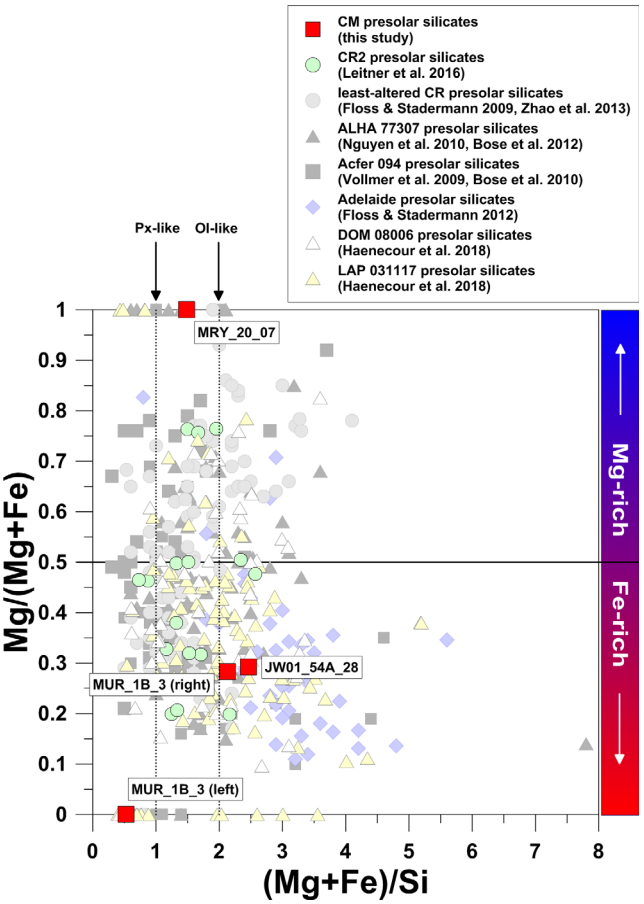

Fig. 9. Mg-Fe-Si element compositions obtained by auger electron spectroscopy for presolar silicates from this study, together with data for silicates from fine-grained (chondrule) rims and interchondrule matrix in the CR2 chondrites GRA 95229 and EET 92161 (light green circles; Leitner et al. 2016), literature data from the minimally altered CR chondrites QUE 99177, MET 00426, and GRV 021710 (gray circles; Floss and Stadermann 2009a; Zhao et al. 2013), the minimally altered C2-ungrouped chondrite Acfer 094 (gray squares; Vollmer et al. 2009; Bose et al. 2010a), the CO3.0 chondrites ALHA77307 (gray triangles; Nguyen et al. 2010; Bose et al. 2012), DOM 08006 (Haenecour et al. 2018), and LAP 031117 (Haenecour et al. 2018), and the C-ungrouped chondrite Adelaide (Floss and Stadermann 2012). Dotted vertical lines denote the compositions of stoichiometric pyroxene ([Mg + Fe]/Si = 1) and olivine ([Mg + Fe]/Si = 2). The horizontal line marks the border between Mg-rich and Fe-rich compositions. (Color figure can be viewed at wileyonlinelibrary.com.)

Origins of Fe-Rich Presolar Dust Grains

Two of the silicate grains studied by AES show comparably high Fe-abundances (12–18 atom%, Table A1 in the Appendix and Fig. 8). This is compatible with the observation that many of the stardust silicates found to date have relatively high Fe contents (Fig. 8), and stands in contrast to equilibrium condensation models predicting silicates with higher Mg contents as the first silicate phases to condense at high temperatures (~1000 K) in stellar environments (Gail 2003; Min et al. 2007). The origin of this Fe is still a matter of intense research, as it may be either a primary condensation or a secondary alteration feature (Floss et al. 2008; Vollmer et al. 2009; Bose et al. 2010a, 2010b; Ong and Floss 2015). One feasible *primary*

mechanism for the production of Fe-rich silicates would be nonequilibrium grain condensation in stellar outflows (see also the discussion in Bose et al. 2010a). Gas and dust are rapidly driven outward by radiation pressure, resulting in a steep temperature drop where equilibrium may not be maintained. This would allow the incorporation of considerable amounts of Fe into condensing silicate grains (Gail and Sedlmayr 1999; Gail 2003). This is further supported by laboratory experiments on nonequilibrium condensation of silicates (Rietmeijer et al. 1999; Nuth et al. 2000), as well as astronomical observations of Fe-rich silicates (e.g., Kemper et al. 2001). The experiments showed that Mg- and Fe-rich condensates with either high Mg- or Fe-contents form directly from the vapor, while grains with intermediate or "mixed" Mg-Fe-compositions are not among the primary condensates (Rietmeijer et al. 1999). Furthermore, Rietmeijer et al. (1999) proposed the accretion of dust aggregates from endmember silicates, which subsequently are transformed by energetic reactions into ferromagnesian grains. Especially the heterogeneous composition of MUR_1B_3 (Si-rich Fe-silicate, together with a fayalite-like, i.e., Fe-rich olivine-like, composition) might be indicative of an origin by nonequilibrium processes (Rietmeijer et al. 1999; Ferrarotti and Gail 2001).

Possible *secondary* processes responsible for the introduction of Fe into presolar grains include Fe ion implantation or preferential sputtering of Mg and Si relative to Fe (e.g., Jones 2000), assuming sufficiently long residence times of the dust grains in the ISM. This might have indeed played a major role for JW01_S4A_28, with its Si-poor- and Fe-rich (Mg# = 29) composition. For MUR_1B_3, however, this effect could only have played a minor role (if any). We would expect a Fe-rich and Si-*poor* composition instead of the Si-rich grain portion, and a rather pyroxene-like composition instead of the Fe-rich olivine-like grain portion (Table A1 in the Appendix), due to the aforementioned preferential removal of Si and Mg compared to Fe by sputtering processes. Secondary parent body processes like aqueous alteration and thermal metamorphism can also be responsible for the introduction of additional Fe via fluid–mineral interactions (Le Guillou et al. 2015; Vollmer et al. 2016; Hopp and Vollmer 2018), or diffusion (Jones and Rubie [1991]; Vollmer et al. [2009] and references therein). Especially for the CM chondrites, there is a growing body of evidence that at least some specimens experienced some degree of thermal metamorphism, in addition to the abundant aqueous alteration (Nagashima et al. 2005; Tonui et al. 2014; Schrader and Davidson 2017; King et al. 2019). Thus, their presolar grain inventory might have also been affected by such processes, resulting in grain destruction and/or chemical modification.

Presolar Fe-oxides are very rare in our current inventory of presolar dust; only a few grains have been observed so far (Floss et al. 2008; Bose et al. 2010a; Zega et al. 2015; Haenecour et al. 2018). Five of them (Bose et al. 2012; Zega et al. 2015; Haenecour et al. 2018) originate from low-mass AGB stars, while three grains (Floss et al. 2008; Bose et al. 2010a) belong to Group 4. Although a supernova origin is now widely accepted for the Group 4 silicate and oxides, Floss et al. (2008) showed that in the case of Fe-oxides, parent stars with supersolar metallicities might well be a viable alternative. A proper elemental quantification of grain JW01_02B_02 by AES was hampered by the fact that, due to the position of the analysis spot, there is an unknown contribution from surrounding Mg- (and potentially Fe-) bearing material (Fig. 6a). Thus, we could not determine whether JW01_02B_02 had a magnetite-, wüstite-, or magnesiowüstite-like composition, although magnesiowüstite appears less likely, judging from the AES element maps. Preparation of the grain for compositional and structural analysis by TEM was not successful, and no further information could be obtained.

As discussed by Floss et al. (2008), condensation of magnesiowüstite (Mg,Fe)O is likely to occur under nonequilibrium conditions around AGB stars with low mass-loss rates ($\dot{M} \leq 4 \times 10^{-6}$ $M_{\odot}yr^{-1}$; Ferrarotti and Gail 2003). Its condensation is prevented at higher rates due to the early condensation of silicates. Calculations by Ferrarotti and Gail (2003) show that with decreasing temperature, higher concentrations of Fe can be incorporated into condensing magnesiowüstite grains; however, formation of almost pure FeO requires an additional explanation. Additional diffusion of Fe into the grain might well explain its composition, although we cannot constrain whether this already happened in the circumstellar envelope, or later on the meteorite parent body. Zega et al. (2015) discussed the formation conditions for circumstellar Fe_3O_4, around AGB stars. They found that oxidation of previously formed Fe dust in the circumstellar envelope is feasible, if residence times of ~9,000–500,000 years are taken into account. However, due to the higher ejection velocities and the resulting faster dispersion of gas and dust in supernova environments, we do not consider such resident times as very likely in the present case. As mentioned earlier, Floss et al. (2008) concluded a more likely origin of their Fe-oxide grain from a high metallicity AGB-star, although its O-isotopic signature would also comply with a CCSN origin. Moreover, there is some observational evidence for the presence of supernova Fe-oxides: In IR spectra from the supernova remnant

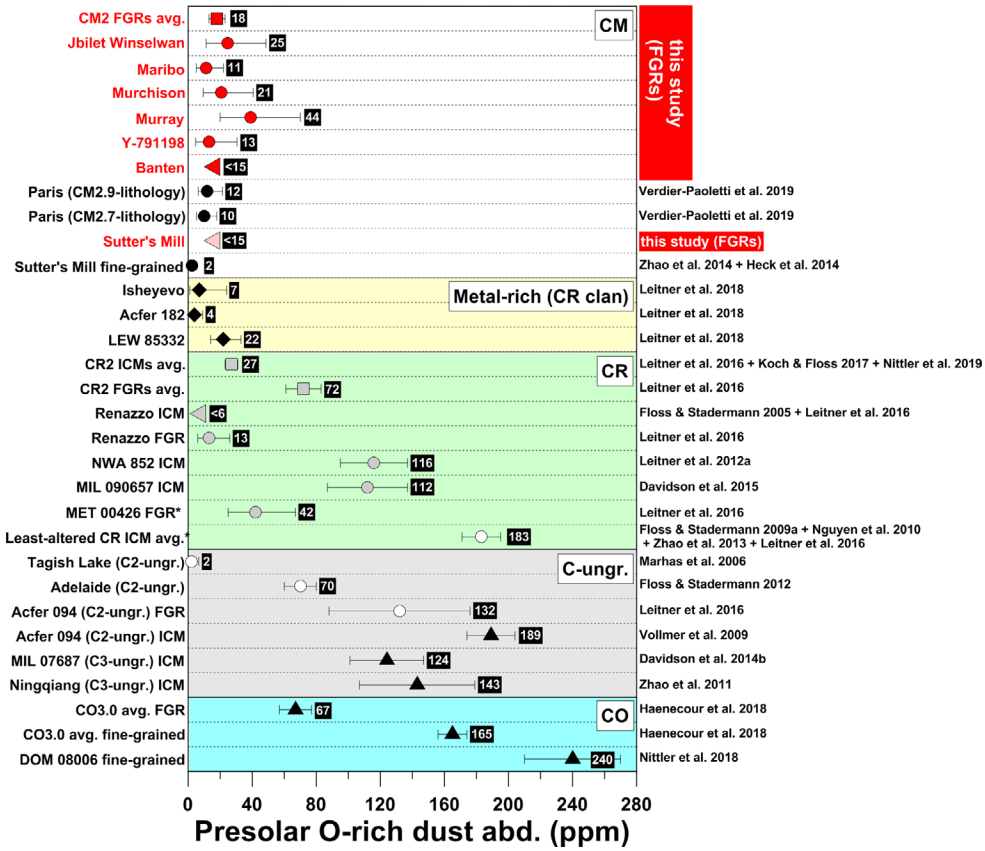

Fig. 9. Abundances of presolar O-rich dust grains in parts per million (ppm) for the CM chondrites and Sutter's Mill from this study. For comparison, literature data for CM, CO, and CR chondrites; clast material from the metal-rich chondrites of the CR clan; as well as several ungrouped carbonaceous chondrites are shown (Floss and Stadermann 2005, 2009a, 2012; Marhas et al. 2006; Vollmer et al. 2009; Nguyen et al. 2010; Mostefaoui 2011; Zhao et al. 2011, 2013, 2014; Leitner et al. 2012a, 2016, 2018; Davidson et al. 2014b, 2015; Heck et al. 2014; Koch and Floss 2017; Haenecour et al. 2018; Nittler et al. 2018, 2019; Verdier-Paoletti et al. 2019a). All errors are 1σ. FGR: fine-grained (chondrule) rim; ICM: interchondrule matrix. *Least altered CRs include the CR2 chondrites MET 00426, QUE 99177, and GRV 021710. (Color figure can be viewed at wileyonlinelibrary.com.)

Cassiopeia A, FeO has been identified as one of the carriers of the 21 μm feature (Rho et al. 2008, 2009; Arendt et al. 2014). Therefore, we can neither confirm nor refute an AGB star or CCSN origin for our grain.

Presolar Grain Abundances and Grain Sizes

The occurrence of presolar grains in the FGRs of the CM chondrites gives evidence for their relatively primitive nature and thus for a nebular origin of the host rims, similar to the FGRs observed in CR (e.g., Leitner et al. 2016) and CO chondrites (e.g., Haenecour et al. 2018). The observed abundances of O-rich presolar grains in the fine-grained chondrule rims in CM chondrites are comparable with both the abundances in the interchondrule matrix (ICM) of moderately altered CR2 chondrites (Leitner et al. 2016; Koch and Floss 2017) and fine-grained clasts of petrologic types 1–2 in three metal-rich chondrites from the CR clan, Isheyevo (CH/CB [high metal/Bencubbin-like] 3), Acfer 182 (CH3), and Lewis Cliff (LEW) 85332 (C3-ungr.; Leitner et al. 2018; Fig. 9). The concentrations are lower than those observed for the FGRs in a set of CR2 chondrites (Leitner et al. 2016), as well as those reported for the least altered chondrites (Floss and Stadermann 2009a; Vollmer et al. 2009; Nguyen et al. 2010; Zhao et al. 2013; Nittler et al. 2018; Fig. 9), which can be attributed to progressive parent body processing. Several classification schemes have been introduced to assign petrologic subtypes to the CM chondrites (Rubin et al. 2007; Alexander et al. 2013; Howard et al. 2015; Table 1). With the exception of Maribo and Sutter's Mill, all CMs studied here span a very narrow range of bulk petrologic subtypes, no matter which classification scheme is used (Table 1). Sutter's Mill experienced more severe alteration (CM2.0-2.1; Jenniskens et al. 2012) and is not considered a "classical" CM, while Maribo is, together

with the CM Paris (Hewins et al. 2014), apparently one of the least altered CMs, with Maribo being >CM2.6 (Haack et al. 2012), and Paris classified as ~CM2.9 (Hewins et al. 2014). The vast majority of CM chondrites are brecciated (Bischoff et al. 2006), complicating the assignation of representative "bulk" petrologic subtypes (Bischoff et al. 2017). However, within error limits, there is no significant difference between the presolar O-rich grain abundances of Maribo and the other CMs investigated here. Moreover, the abundances determined for two lithologies from Paris (Verdier-Paoletti et al. 2019a; Fig. 9) also lie within the average range of abundances determined for the CMs (Fig. 9). Thus, the presolar silicate and oxide inventories of even the least altered CMs are significantly affected by aqueous alteration (and, potentially, by thermal metamorphism), if we assume a largely homogeneous initial distribution of presolar silicates and oxides in the protosolar nebula. Alternatively, given the relatively primitive nature of Paris and Maribo, the precursor material of their matrices could have contained a smaller initial abundance of presolar O-rich grains than the fine-grained materials accreted, for example, into CR or CO chondrites. This could have been the result of anisotropies/heterogeneities in the distribution of presolar O-rich dust in the formation region of the Sun, depending on how well mixed the precursor material of the prestellar core was. And since oxygen-rich and carbonaceous dust form during different evolutionary stages of AGB stars, they might as well experience differing degrees of mixing in the ISM. Moreover, silicates (and oxides) must not necessarily form around every evolved star, while model calculations indicate that the vast majority of low-mass AGB stars undergo C-rich episodes with dust formation. This could hypothetically result in localized "clumps" or "bubbles" with O-rich and C-rich dust. With greatly enhanced statistics, future studies might be able to monitor differences in the presolar grain concentrations of samples with different petrologic subtypes. The presolar SiC abundances of our CM samples do not differ significantly from the literature values obtained by ion imaging (Table 3; Fig. 10), supporting the idea of a roughly homogeneous distribution of SiC in primitive solar system materials (Davidson et al. 2014a). However, a potential bias might be introduced by the applied method of SiC detection by targeting ^{28}Si-hotspots recorded during the O isotope analyses (see the Methods section). Smaller grains might have been missed; thus, the abundance might have been underestimated, but the preferential detection of larger grains could have an opposing effect by leading to overestimating the true abundances.

Presolar silicate grains are considered to be more susceptible to aqueous alteration than the more refractory Al-oxide grains (Floss and Stadermann 2009a; Leitner et al. 2012a); thus, the presolar silicate abundances as well as the presolar silicate/oxide (sil./ox.) ratios of primitive materials can provide information on the degree of alteration they experienced. While high sil./ox. ratios would thus indicate relatively unaltered material, lower ratios would be found for more aqueously altered host material, due to preferential destruction of presolar silicate grains in comparison to the more refractory species, such as Al-rich oxides or SiC. In the vast majority of cases, the number of presolar oxide grains found in individual meteorites is very low (typically <5), resulting in relative errors of >50% for the respective sil./ox. ratios, making them practically useless to monitor none but the most extreme differences in the degrees of aqueous alteration between individual meteorites (i.e., in cases where very low sil./ox. ratios would be observed alongside sufficiently high ratios, depending on the respective statistics). The presolar silicate/oxide ratio of the CM chondrites studied here stands out, because it is the lowest ratio observed so far (sil./ox. = 1.5), only comparable with the ratio of ~2 found for the CR2 chondrite NWA 852 (Leitner et al. 2012a). Surprisingly, the presolar O-rich grain inventories of the ICM of other CR2 chondrites and the hydrated lithic clasts in the CH/CB chondrites (Leitner et al. 2016, 2018; Koch and Floss 2017; Nittler et al. 2019) are dominated by silicates, although the presolar grain abundances are similar to the CM chondrites studied here (Fig. 11). Both the CM and CR chondrites are generally classified as petrologic type 2, but several classification schemes have been proposed to define suitable petrologic subtypes. The studies by Alexander et al. (2013) and Howard et al. (2015) both introduce a petrologic subtype scale that allows such an intergroup comparison for the CMs and CRs, based on the bulk water/OH H content. For the CM2 chondrites of our study, petrologic subtypes range from 1.5 to 1.7 on these scales (for Maribo and Sutter's Mill, no subtype has been determined yet). For the CR2 chondrites, the values are typically higher, ranging from 2.4 to 2.8 (with the exception of Al Rais with 2.0), and for the C3-ungrouped LEW 85332 (which belongs to the metal-rich chondrites of the CR clan and whose presolar grain inventory was studied by Leitner et al. 2018), 2.3 is calculated. These results illustrate the general trend quite well (CM2s are more altered than CR2s, the fine-grained clasts in the CH and CB chondrites and in LEW 85332 are also of petrologic types 1–2). However, there are some issues with the subtypes assigned to the CR chondrites; Renazzo is more severely altered than

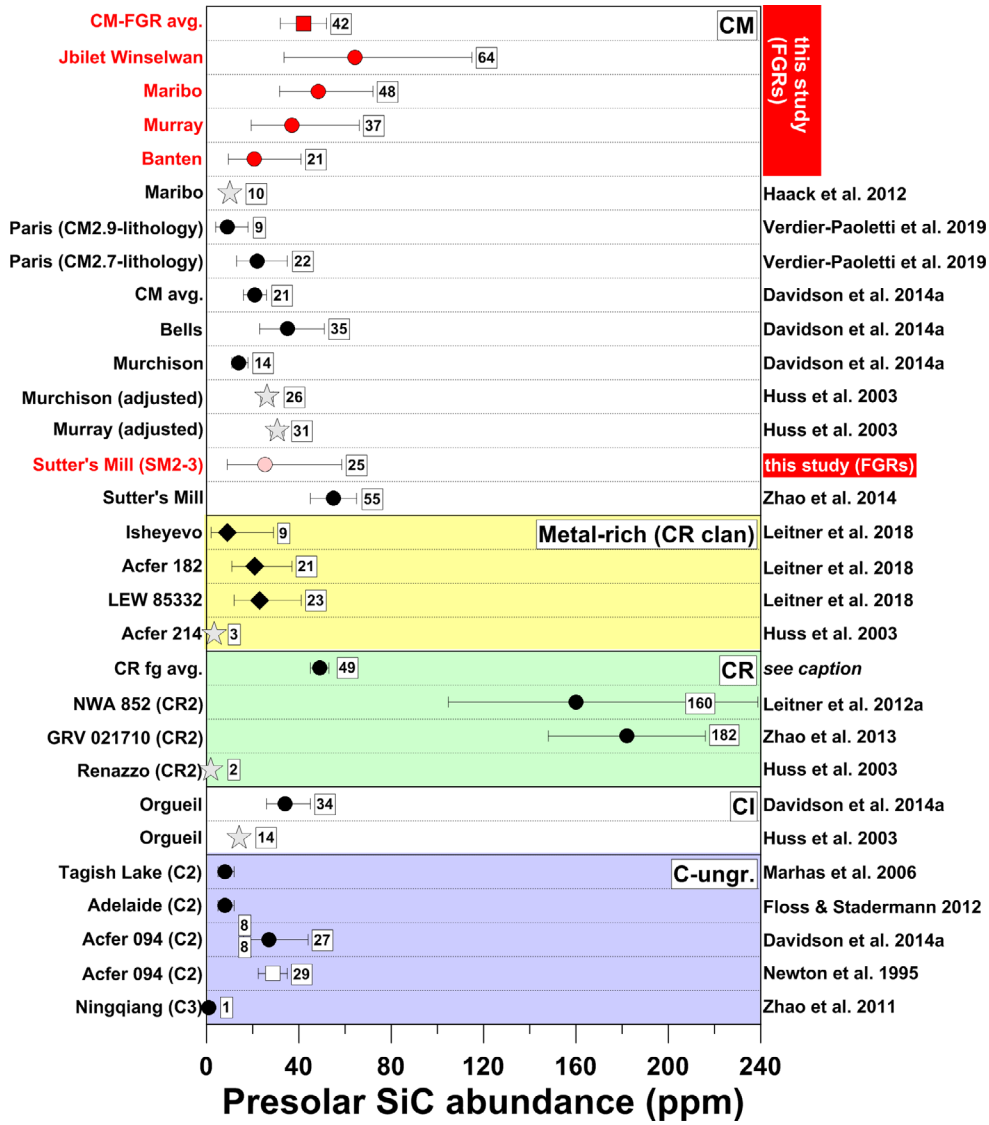

Fig. 10. Abundances of presolar SiC grains in parts per million (ppm) for the CM chondrites and Sutter's Mill from this study. For comparison, literature data for CM and CR chondrites, clast material from the metal-rich chondrites of the CR clan, Orgueil (CI1), and a set of ungrouped carbonaceous chondrites are shown (Marhas et al. 2006; Zhao et al. 2011, 2013, 2014; Floss and Stadermann 2012; Leitner et al. 2012a, 2018; Davidson et al. 2014a, 2015; Verdier-Paoletti et al. 2019a; the "CR fg (fine-grained) average" was calculated with data from Floss and Stadermann 2005, 2009b; Nguyen et al. 2010; Leitner et al. 2012c; Davidson et al. 2014a, 2015). Data are from ion imaging surveys except for the star symbols (abundances inferred from noble gas analyses, Huss et al. 2003; Haack et al. 2012) and the white square symbol (data from stepped combustion measurements, Newton et al. 1995). All errors are 1σ. FGR: fine-grained rims. (Color figure can be viewed at wileyonlinelibrary.com.)

most of the Antarctic CR2s and has an average ICM abundance of <6 ppm for O-rich presolar grains (Fig. 9), but has a higher petrologic classification than QUE 99177 with an average ICM abundance of 177 ppm for O-rich presolar grains. There is a discussion of these issues in Alexander et al. (2013) and Leitner et al. (2016), and one of the major reasons for these discrepancies might be the fact that aqueous alteration on the respective parent bodies did not occur homogeneously, both in spatial distribution and temperature. Another major reason could be that assigning bulk petrologic types to these rocks is difficult, since both CM and CR chondrites are highly brecciated (Bischoff et al. 2006, 2017). While different degrees of aqueous alteration would explain *decreasing* presolar silicate abundances *in combination* with decreasing sil./ox. ratios, we found abundances *similar* to those found for the ICM of CR2s and the matrix

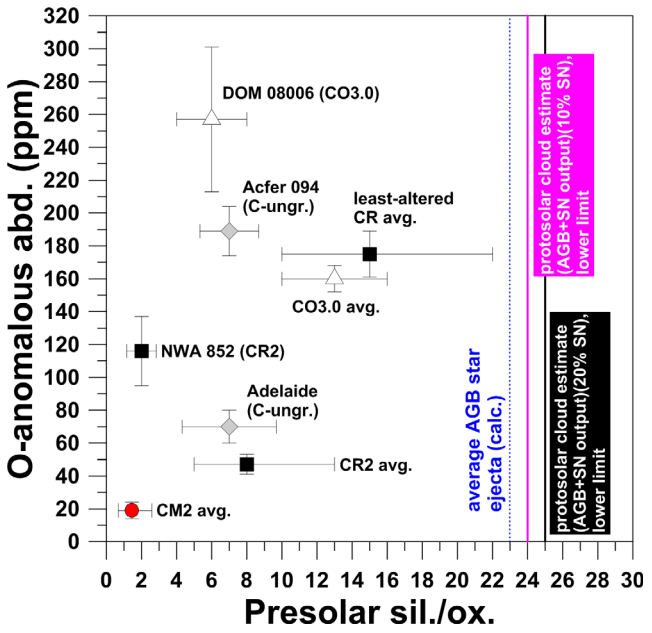

Fig. 11. Presolar silicate/oxide ratios (calculated from the respective presolar grain abundances) plotted versus the presolar O-anomalous grain abundances for the CM2 chondrites of this study (average). For comparison, data for the average from a set of CR2 chondrites (Leitner et al. 2016) and "least altered" CR chondrites (Floss and Stadermann 2009a; Nguyen et al. 2010; Zhao et al. 2013; Leitner et al. 2016) are shown, as well as an average value for CO3.0 chondrites (Nguyen et al. 2010; Bose et al. 2012; Haenecour et al. 2018), together with ratios for several individual carbonaceous chondrites: Adelaide (C-ungrouped, Floss and Stadermann 2012), NWA 852 (CR2, Leitner et al. 2012a), Acfer 094 (C-ungrouped, Vollmer et al. 2009), and DOM 08006 (CO3.0, Nittler et al. 2018). All errors are 1σ. The vertical dotted blue line denotes the theoretical sil./ox. ratio estimated for AGB star ejecta (from Leitner et al. 2012a); the magenta and black solid lines mark the sil./ox. estimate for the protosolar molecular cloud, with 10% and 20% supernova contribution added, respectively. (Color figure can be viewed at wileyonlinelibrary.com.)

clasts in the metal-rich chondrites together, but with *different* sil./ox. ratios.

This could indicate a heterogeneous distribution of presolar silicates and oxides within the carbonaceous chondrite forming regions. For a clear conclusion, improved statistics are needed (especially on the presolar oxide abundances). Poor statistics for presolar oxides is a critical issue, but if we focus on the few primitive chondrites with better constrained sil./ox. ratios (NWA 852, Adelaide, Acfer 094, DOM 08006; Vollmer et al. 2009; Floss and Stadermann 2012; Leitner et al. 2012a; Nittler et al. 2018), and combine the results from multiple studies of the most primitive CR and CO chondrites (Fig. 9), we find a relatively large spread between the individual data points. Due to the large statistical errors of some of the sil./ox. ratios considered here, the ratios are comparable to one another within 2 sigma-errors. Thus, it is still possible that with improved statistics, it will be possible to show that there is no significant variation in the sil./ox. ratios of different meteorite groups or individual meteorites. This would indicate a homogeneous distribution of presolar silicates and oxides in the protosolar nebula, that is, the circumstellar dust component had been well mixed in the ISM. However, if further investigations established more significant differences between individual meteorites or groups of meteorites, a potential reason for such heterogeneities is discussed the following paragraph.

An observational study by Karovicova et al. (2013) reported different dust shell structures around four O-rich AGB stars: two stars displayed only features of Al-oxide dust, one star featured a silicate dust shell, and the fourth star had both Al-oxide and silicate shells. Of course, the statistics are not (yet) significant, but it might be a first hint for a larger initial variation of circumstellar sil./ox. ratios, and therefore, the distributions of presolar silicates and oxides in the ISM and also the protosolar cloud might have been less homogeneous than originally anticipated. In a previous study (Leitner et al. 2012a), we estimated a presolar sil./ox. ratio for the presolar dust component in the following way: We assumed (as a first-order approximation) that (during the formation of O-rich dust) almost all Si from AGB stars (which contributed ~90% of the O-rich presolar dust to the protosolar nebula) condenses into silicate dust, while essentially all Al forms oxide dust. SiC and other carbonaceous presolar phases can be neglected at this point, since they form in another stellar evolutionary phase. If we choose pyroxene as silicate proxy and alumina (Al_2O_3) as proxy for oxides, and further consider solar abundances for Al and Si (Asplund et al. 2009, we find a sil./ox. ratio for AGB star dust of Si/(Al/2) = 2 × Si/Al = 23. Of course, the sil./ox. ratio of SN dust has to be considered, too. For a more accurate estimate, we investigated CCSN models from Rauscher et al. (2002) and Pignatari et al. (2016) with stellar masses of 15, 20, 25, 32, and 60 $M_\odot$ and calculated the ratios in the same way. The sil./ox. ratios range from 34 to 230, and as a consequence, we find lower limits for the "protosolar cloud initial" (pci) of 24 (with 10% SN contribution) and 25 (with 20% SN contribution; Fig. 11). However, this first-order approximation might be too simple by adopting a *single* presolar sil./ox. ratio, and the dust in the protosolar cloud might have consisted therefore of several heterogeneously distributed populations with different ratios.

We also observed a slightly larger average grain size (~330 nm) than for the presolar silicates and oxides in

Table 4. Average grain sizes for both the presolar O-rich and silicon carbide grains identified in this study, together with average grain sizes for other chondrites calculated from literature data (with the exception of the data from Davidson et al. (2014a); here, the average grain sizes and standard deviations were directly adapted from the source). For each value, the standard deviation and the number of grains used to calculate the average are given.

	Grain size (avg.) (nm)	Standard dev. (nm)	# grains	References
O-rich grains				
CM avg.	330	115	15	This study
CR avg.	270	80	246	Floss and Stadermann (2009a); Nguyen et al. (2010); Leitner et al. (2012a), Leitner et al. (2016); Zhao et al. (2013)
CH/CB clasts	275	80	11	Leitner et al. (2018)
CO avg.	260	90	331	Nguyen et al. (2010); Bose et al. (2012); Haenecour et al. (2018); Nittler et al. (2018)
Acfer 094 (C2-ungr.)	270	100	218	Vollmer et al. (2009); Bose et al. (2010a); Kodólanyí et al. (2014); Leitner et al. (2016)
SiC grains				
CM avg.	335	100	21	This study
Murchison (CM2)	330	110	16	Davidson et al. (2014a)
Bells (CM2-an.)	770	155	8	Davidson et al. (2014a)
Sutter's Mill	360	155	28	Zhao et al. (2014)
CR avg.	410	115	114	Davidson et al. (2014a)
CR avg.	250	125	92	Floss and Stadermann (2009b); Nguyen et al. (2010); Leitner et al. (2012a); Zhao et al. (2013)
CR-clan metal-rich	380	70	9	Leitner et al. (2018)
Orgueil (CI1)	370	75	13	Davidson et al. (2014a)
CO3.0 avg.	250	105	44	Nguyen et al. (2010); Bose et al. (2012); Nittler et al. (2018)
ALHA77307 (CO3.0)	430	80	11	Davidson et al. (2014a)
Acfer 094 (C2-ungr.)	490	120	5	Davidson et al. (2014a)
RBT 04133 (CV3)	300	65	3	Davidson et al. (2014a)
Semarkona (LL3.0)	420	70	7	Davidson et al. (2014a)

the CM suite of meteorites compared to other chondrites (260–270 nm). For comparison with the presolar grain sizes from other chondrites and chondrite groups (Table 4), we only considered reference data from studies conducted with the "standard" NanoSIMS settings (spatial resolution ≥100 nm). The recent investigations of Hoppe et al. (2015, 2017) used a higher spatial resolution (<100 nm), detecting a multitude of smaller (d < 150 nm) grains that are typically missed in lower resolution mode, and thus are not directly comparable with the results from other studies. Additional uncertainty arises from the fact that the diameters for many grains have been determined from NanoSIMS ion images, since different laboratories and researchers might well apply differing methods or criteria when estimating the size of a presolar grain. Unfortunately, we currently see no way to eliminate this potential systematical error. However, we have at least the possibility to use an "internal" calibration to compare the grain sizes of the presolar O-rich grains from the CM chondrites with data from studies conducted at the MPIC (Vollmer et al. 2009; Leitner et al. 2012a, 2016, 2018; Kodólanyí et al. 2014). The average grain sizes from these "calibration studies" do not differ significantly from the averages found in other studies (Table 4) and are all smaller than the average value calculated for the CM chondrite grains. Moreover, many reported grain sizes are obtained from SEM or AES measurements and thus are more precise than the NanoSIMS-derived. Thus, the best way to get a "reliable" average grain size might be by integrating over a *large* number of grains from *different* studies. The larger average grain size of silicates from this study could be attributed to preferential destruction of smaller grains by progressing aqueous alteration. Al-oxides are generally considered to be largely unaffected by aqueous processes. The majority of presolar Al_2O_3 grains are (thermally stable) α-Al_2O_3 (corundum), but, for example, amorphous alumina has also been observed (Stroud et al. 2004). To our knowledge, no investigations have been conducted on α-Al_2O_3, but it has been shown that contact of water with (metastable) γ-Al_2O_3 leads to hydration/hydroxylation and, subsequently, to formation of Al-oxihydroxides and Al-hydroxides at the Al_2O_3-surface; moreover, the pH value of the liquid has a strong influence on the speed

of the respective reactions (e.g., Lefèvre et al. 2002). Of course, we do not have exact information on the fluid interaction processes affecting the fine-grained CM constituents; however, this could be a possible scenario for the destruction of (smaller) amorphous Al-oxides. Some CM chondrites, including Jbilet Winselwan, Murchison, and Murray appear to have experienced thermal metamorphism to a certain degree (Nagashima et al. 2005; Tonui et al. 2014; Schrader and Davidson 2017; King et al. 2019), which could also have contributed to the preferential destruction of smaller grains. Reported peak metamorphic temperatures are relatively low: T < 220 °C–230 °C for Murray and Murchison (Schrader and Davidson 2017), and up to 400 °C–500 °C for some lithologies in Jbilet Winselwan (King et al. 2019). However, these temperatures are typically determined by investigating chondrules and other similarly large mineral grains; the thermal effects and peak temperatures experienced by the fine-grained matrix (which hosts the presolar grains) might be much stronger: Bland et al. (2014) showed in their study that low-energy impacts have the potential to cause strong temperature increases of even more than 1000 K in localized areas in the fine-grained fraction of chondrites, while larger and compact constituents like chondrules would act as heat sinks and not be affected in the same way as the matrix. Evidence for multiple of such low-energy impacts has been found in CM chondrites (Lindgren et al. 2015); thus, presolar grain destruction by these events is a possible scenario that might be responsible for the observed presolar silicate and oxide abundances.

If we do a first-order estimate of the "pre-alteration" presolar silicate abundance, similar to the calculation made by Leitner et al. (2012a), but remembering that the scenario is likely more complicated, we find an estimated concentration of 170 (+130/–90) ppm in the CMs, much lower than the estimate of ~800 ppm made for NWA 852 (CR2). We calculated these "pre-alteration" abundances by using the respective sil./ox. ratios and the "(pci)" ratio estimated above as calibration factors for the presolar silicate abundances: $([\text{sil./ox.}]_{\text{pci}}/[\text{sil./ox}]_{\text{meteorite}})\times (\text{presolar silicate abundance})_{\text{meteorite}}$. However, if we consider the different average grain sizes, the abundance must be adjusted: Amari et al. (1994) found that the grain size distribution of presolar SiC and graphites from grain separates follow a log-normal distribution and drew the conclusion that this was the preferred distribution law for grain formation in circumstellar envelopes, possibly reflecting a two-stage process of grain evolution by evaporation and recondensation. However, it has to be taken into account that the heavy processing necessary to produce these grain separates could have led to the destruction of smaller grains, and thus, the observed distribution might not be representative. Therefore, we apply here the MRN model distribution found for interstellar grains (Mathis et al. 1977), where the abundance scales with $a^{-3.5}$ ("a" being the grain radius) to the presolar silicates and oxides. We find that 260 nm grains are predicted to be 2.3 times more abundant than 330 nm grains. With this correction factor, the estimate for presolar silicates becomes 400 (+300/–200) ppm, which overlaps, within error limits, with the ~800 (±340) ppm for NWA 852, and lies also in the range observed for primitive IDPs (Floss et al. 2006; Busemann et al. 2009; Davidson et al. 2012).

The size distributions of the SiC grains in the CMs agree within error limits with the size distributions observed in other studies for Murchison, Sutter's Mill, metal-rich chondrites from the CR clan, and Orgueil (CI; Table 4). The average from the anomalous CM Bells is significantly larger (770 ± 155 nm), but this is addressed in the original study by Davidson et al. (2014a). For the CR chondrites, we find a difference between the average determined by Davidson et al. (2014a) from 114 grains, and the average calculated from a set of other studies (Floss and Stadermann 2009b; Nguyen et al. 2010; Leitner et al. 2012a; Zhao et al. 2013) for 92 grains: 410 ± 155 nm versus 250 ± 125 nm, that is, the size ranges still overlap. The CO average calculated from Nguyen et al. (2010), Bose et al. (2012), and Nittler et al. (2018) is with 250 ± 105 nm also smaller than the CM average, while the values for a set of individual chondrites ([ALHA77307 CO3.0], Acfer 094 [C2-ungr.], RBT 04133 [CV3], Semarkona [LL3.0]) from Davidson et al. (2014a) range from 300 ± 65 nm to 490 ± 120 nm. Despite this relative scatter of the average values, the size ranges still overlap. Currently, we cannot resolve if the observed differences are indicative of a small difference in the respective grain sizes, or are mainly the result of different approaches of determining grain sizes, as discussed earlier in this manuscript. At least, our method of targeting ^{28}Si-hotspots could have introduced a bias toward larger SiC grains, since smaller ones (whose ^{28}Si intensities might be not as pronounced the signal from matrix silicates) might have been missed. However, this does not necessarily refute size-sorting of grains taking place in the solar nebula, since the presolar SiCs seem to have slightly larger average sizes than the silicates and oxides, and thus simply were not affected. However, it is interesting to note that for the various SiC *grain separates* that were studied over the years, a general difference between the average grain sizes of SiC from Murchison and other primitive meteorites was observed (Huss et al. 1997; Russell et al.

1997; Zinner et al. 2006). At a first glance, this stands in contradiction to our observations for the SiC in CM chondrites, and also to the findings of Davidson et al. (2014a) for SiC from the Murchison meteorite. However, this discrepancy can be explained by the still limited statistics on SiC from in situ investigations compared to the grains isolated from grain separates and the fact that for in situ ion imaging studies, typically, fine-grained areas are targeted, so that larger SiCs in coarser grained regions might be missed. Davidson et al. (2014a) conducted their study on presolar SiC contained in extracted insoluble organic matter, and not on meteorite thin sections. Therefore, such a potential bias should not have affected their measurements. However, if we apply again the MRN model distribution from Mathis et al. (1977), we find that for 16 SiC grains of ~330 nm (as reported by Davidson et al. 2014a), ~0.33 grains of 1 μm would be expected statistically. From this number, it can easily be seen that the grain statistics needs to be improved significantly for proper conclusions.

SUMMARY AND CONCLUSIONS

1. We conducted an investigation of the presolar grain (silicates, oxides, and SiC) inventories in the FGRs of a set of CM chondrites and the CM-related carbonaceous chondrite Sutter's Mill. Presolar O-rich grains (silicates and oxides) are significantly less abundant (18 ± 5 ppm) in the fine-grained rims of the CM chondrites than in the fine-grained rims of CR2 chondrites (72 ± 13 ppm; Leitner et al. 2016) and also the fine-grained components of the most pristine chondrites (CO3.0, minimally altered CR2, Acfer 094; Nguyen et al. 2007, 2010; Floss and Stadermann 2009a; Vollmer et al. 2009; Bose et al. 2010a, 2012; Zhao et al. 2013; Leitner et al. 2016; Haenecour et al. 2018; Nittler et al. 2018). The concentrations are, however, compatible with those determined for the interchondrule matrix material of a set of CR2 chondrites (Floss and Stadermann 2005; Leitner et al. 2016; Koch and Floss 2017) and hydrated lithic clasts from Acfer 182 (CH3), Isheyevo (CH/CB3), and LEW 85332 (C3-ungr.; Leitner et al. 2018). The hydrated state of the FGR material in CM CCs suggests destruction of a significant fraction of the original O-rich presolar grain population, indicating a degree of alteration similar to more severely altered CRs like Renazzo, and the hydrated clasts in the CH/CB chondrites.
2. The CM chondrites have the lowest presolar silicate/oxide ratio (~1.5) observed so far for primitive solar system materials. This may result from the destruction of presolar silicates by more severe aqueous alteration, but the lack of clear correlation between sil./ox. ratios and presolar O-rich grain abundances could indicate an inherently heterogeneous distribution of silicate and oxide stardust in the protosolar cloud. This is in contrast with the relatively homogeneous distribution of presolar SiC inferred by Davidson et al. (2014a).
3. There is some evidence for slightly larger average grain sizes of presolar silicates and oxides in the CM chondrites compared to the grain inventories of other chondrites. In contrast, for the SiC population, we observed no significant difference from the average grain sizes of other chondrites, although the data appear to indicate a larger scatter than observed for the O-rich grains. Better statistics are needed, but the size difference could be indicative of a heterogeneous size distribution among the silicate and oxide stardust in the solar system. Alternatively, the larger grain sizes could result from preferential destruction of smaller grains by thermal metamorphism (and potentially aqueous alteration, depending on the chemical environment) experienced by the CM chondrites, while the SiC grains were less affected, due to higher thermal stability.
4. The range of Fe-contents observed in four presolar silicate grains corresponds with the range observed for the CR and CO3.0 chondrites, and the ungrouped minimally altered C2-chondrite Acfer 094. One large silicate from Jbilet Winselwan is crystalline, and is likely åkermanite (Mg-rich melilite), or an åkermanite-diopside composite.
5. The presence of presolar dust in the FGRs of CM chondrites studied here gives evidence for a nebular origin of the host rims, similar to the FGRs observed in CR (Leitner et al. 2016) and CO chondrites (Haenecour et al. 2018).

Acknowledgments—JL, PH, KM, and CV acknowledge support by the DFG through SPP 1385 "The first ten million years of the solar system—a planetary materials approach" (by grants HO 2163/1-2, LE 3279/1-1, and VO1816/1-1). The Auger nanoprobe work was supported by NASA grants NNX12AN77H (P. Haenecour) and NNX14AG25G (C. Floss). The FIB and TEM facilities at FSU Jena are supported by the DFG through a grant to F. Langenhorst (LA 830/14-1). We thank Elmar Gröner for technical support on the NanoSIMS; Joachim Huth and Antje Sorowka for help with the SEM analyses; Maik Biegler for preparation of the Murchison, Murray, and Jbilet Winselwan samples; Addi Bischoff from the Institute for Planetology in Münster for making the Maribo and Sutter's Mill samples available; and the National Institute of Polar

Research in Japan for providing the Y-791198 sample. We appreciate the constructive reviews by Ann Nguyen, Maitrayee Bose, a third anonymous reviewer, and the associate editor Larry Nittler, which have improved the quality of the manuscript. This research has made use of NASA's Astrophysics Data System.

Editorial Handling—Dr. Larry Nittler

REFERENCES

Alexander C. M. O'D., Howard K. T., Bowden R., and Fogel M. L. 2013. The classification of CM and CR chondrites using bulk H, C and N abundances and isotopic compositions. *Geochimica et Cosmochimica Acta* 123:244–260.

Amari S., Anders E., Virag A., and Zinner E. 1990. Interstellar graphite in meteorites. *Nature* 345:238–240.

Amari S., Lewis R. S., and Anders E. 1994. Interstellar grains in meteorites: I. Isolation of SiC, graphite, and diamond; size distributions of SiC and graphite. *Geochimica et Cosmochimica Acta* 58:459–470.

Amari S., Nittler L. R., and Zinner E. 2001. Presolar SiC grains of type A nd B: Their isotopic compositions and stellar origins. *The Astrophysical Journal* 559:463–483.

Arendt R. G., Dwek E., Kober G., Rho J., and Hwang U. 2014. Interstellar and ejecta dust in the Cas A supernova remnant. *The Astrophysical Journal* 786:55–76.

Asplund M., Grevesse N., Sauval J. A., and Scott P. 2009. The chemical composition of the Sun. *Annual Review of Astronomy and Astrophysics* 47:481–522.

Bernatowicz T., Fraundorf G., Tang M., Anders E., Wopenka B., Zinner E., and Fraundorf P. 1987. Evidence for interstellar SiC in the Murray carbonaceous meteorite. *Nature* 330:728–730.

Bischoff A., Scott E. R. D., Metzler K., and Goodrich C. A. 2006. Nature and origins of meteoritic breccias. In *Meteorites and the early solar system II*, edited by Lauretta D. S. and McSween H. Y. Jr. Tucson, Arizona: University of Arizona Press. pp. 679–712.

Bischoff A., Ebert S., Metzler K., and Lentfort S. 2017. Breccia classification of CM chondrites (abstract #6089). *Meteoritics & Planetary Science* 52:A26.

Bland P. A., Stadermann F. J., Floss C., Rost D., Vicenzi E. P., Kearsley A. T., and Benedix G. K. 2007. A cornucopia of presolar and early solar system materials at the micrometer size range in primitive chondrite matrix. *Meteoritics & Planetary Science* 42:1417–1427.

Bland P. A., Collins G. S., Davison T. M., Abreu N. M., Ciesla F. J., Muxworthy A. R., and Moore J. 2014. Pressure-temperature evolution of primordial solar system solids during impact-induced compaction. *Nature Communications* 5:5451–5463.

Boothroyd A. I. and Sackmann I.-J. 1999. The CNO isotopes: Deep circulation in red giants and first and second dredge-up. *The Astrophysical Journal* 510:232–250.

Bose M., Floss C., and Stadermann F. J. 2010a. An investigation into the origin of Fe-rich presolar silicates in Acfer 094. *The Astrophysical Journal* 714:1624–1636.

Bose M., Zhao X., Floss C., Stadermann F. J., and Lin Y. 2010b. Stardust material in the paired enstatite chondrites: SAH 97096 and SAH 97159. Proceedings of the 11th Symposium on Nuclei in the Cosmos, July Heidelberg, Germany. http://pos.sissa.it/archive/conferences/100/138/NIC%20XI_138.pdf

Bose M., Floss C., Stadermann F. J., Stroud R. M., and Speck A. K. 2012. Circumstellar and interstellar material in the CO3 chondrite ALHA77307: An isotopic and elemental investigation. *Geochimica et Cosmochimica Acta* 93:77–101.

Brearley A. J. and Jones R. H. 1998. Chondritic meteorites. In *Reviews in mineralogy: Planetary materials*, edited by Papike J. J. Washington, D.C.: Mineralogical Society of America. pp. 313–398.

Busemann H., Nguyen A. N., Cody G. D., Hoppe P., Kilcoyne A. L. D., Stroud R. M., Zega T. J., and Nittler L. R. 2009. Ultra-primitive interplanetary dust particles from the comet 26P/Grigg–Skjellerup dust stream collection. *Earth and Planetary Science Letters* 288:44–57.

Chizmadia L. J. and Brearley A. J. 2008. Mineralogy, aqueous alteration, and primitive textural characteristics of fine-grained rims in the Y-791198 CM2 carbonaceous chondrite: TEM observations and comparison to ALHA81002. *Geochimica et Cosmochimica Acta* 72:602–625.

Choi B.-G., Huss G. R., Wasserburg G. J., and Gallino R. 1998. Presolar corundum and spinel in ordinary chondrites: Origins from AGB stars and a supernova. *Science* 282:1284–1289.

Choi B.-G., Wasserburg G. J., and Huss G. R. 1999. Circumstellar hibonite and corundum and nucleosynthesis in asymptotic giant branch stars. *The Astrophysical Journal* 522:L133–L136.

Ciesla F. J., Lauretta D. S., Cohen B. A., and Hood L. L. 2003. A nebular origin for chondritic fine-grained phyllosilicates. *Science* 299:549–552.

Cuzzi J. N. 2004. Blowing in the wind: III. Accretion of dust rims by chondrule-sized particles in a turbulent protoplanetary nebula. *Icarus* 168:484–497.

Davidson J. 2009. NanoSIMS and beyond: presolar grains in primitive materials and solar system formation. PhD dissertation. Open University, Milton Keynes, UK.

Davidson J., Busemann H., and Franchi I. A. 2012. A NanoSIMS and Raman spectroscopic comparison of interplanetary dust particles from comet Grigg-Skjellerup and non-Grigg Skjellerup collections. *Meteoritics & Planetary Science* 47:1748–1771.

Davidson J., Busemann H., Nittler L. R., Alexander C. M. O'D., Orthous-Daunay F.-R., Franchi I. A., and Hoppe FP. 2014a. Abundances of presolar silicon carbide grains in primitive meteorites determined by NanoSIMS. *Geochimica et Cosmochimica Acta* 139:248–266.

Davidson J., Nittler L. R., Alexander C. M. O'D., and Stroud R. M. 2014b. Presolar materials and nitrogen isotope anomalies in the unique carbonaceous chondrite Miller Range 07687 (abstract #1376). 45th Lunar and Planetary Science Conference. CD-ROM.

Davidson J., Alexander C. M. O'D., Schrader D. L., Nittler L. R., and Bowden R. 2015. Miller Range 090657: A very pristine Renazzo-like (CR) carbonaceous chondrite (abstract #1603). 46th Lunar and Planetary Science Conference. CD-ROM.

El Eid M. F. 1994. CNO isotopes in red giants: Theory versus observations. *Astronomy and Astrophysics* 285:915–928.

Ferrarotti A. S. and Gail H.-P. 2001. Mineral formation in stellar winds. II. Effects of Mg/Si abundance variations on

dust composition in AGB stars. *Astronomy and Astrophysics* 371:133–151.
Ferrarotti A. S. and Gail H.-P. 2003. Mineral formation in stellar winds. IV. Formation of magnesiowüstite. *Astronomy and Astrophysics* 398:1029–1039.
Floss C. 2018. Auger spectroscopy in planetary science: Elemental analysis of presolar silicate grains. *Microscopy Today* 26:12–17.
Floss C. and Haenecour P. 2016. Presolar silicate grains: Abundances, isotopic and elemental compositions, and the effects of secondary processing. *Geochemical Journal* 50:3–25.
Floss C. and Stadermann F. J. 2005. Presolar (circumstellar and interstellar) phases in Renazzo: The effects of parent body processing (abstract #1390). 36th Lunar and Planetary Science Conference. CD-ROM.
Floss C. and Stadermann F. J. 2009a. Auger Nanoprobe analysis of presolar ferromagnesian silicate grains from primitive CR chondrites QUE 99177 and MET 00426. *Geochimica et Cosmochimica Acta* 73:2415–2440.
Floss C. and Stadermann F. J. 2009b. High abundances of circumstellar and interstellar C-anomalous phases in the primitive CR2 chondrites QUE 99177 and MET 00426. *The Astrophysical Journal* 697:1242–1255.
Floss C. and Stadermann F. J. 2012. Presolar silicate and oxide abundances and compositions in the ungrouped carbonaceous chondrite Adelaide and the K chondrite Kakangari: The effects of secondary processing. *Meteoritics & Planetary Science* 47:992–1009.
Floss C., Stadermann F. J., Bradley J. P., Dai Z. R., Bajt S., Graham G., and Lea A. S. 2006. Identification of isotopically primitive interplanetary dust particles: A NanoSIMS isotopic imaging study. *Geochimica et Cosmochimica Acta* 70:2371–2399.
Floss C., Stadermann F. J., and Bose M. 2008. Circumstellar Fe oxide from the Acfer 094 carbonaceous chondrite. *The Astrophysical Journal* 672:1266–1271.
Fuchs L. H., Olsen E., and Jensen K. J. 1973. Mineralogy, crystal chemistry and composition of the Murchison (C2) meteorite. *Smithsonian Contributions to the Earth Sciences* 10:399.
Fujiya W., Hoppe P., Zinner E., Pignatari M., and Herwig F. 2013. Evidence for radiogenic sulfur-32 in type AB presolar silicon carbide grains? *The Astrophysical Journal* 776:L29–L34.
Gaffey M. J., Burbine T. H., and Binzel R. P. 1993. Asteroid spectroscopy: Progress and perspectives. *Meteoritics* 28:161–187.
Gail H.-P. 2003. Formation and evolution of minerals in accretion disks and stellar outflows. In *Astromineralogy*., edited by Hennig T. Lecture Notes in Physics 609 Heidelberg: Springer. pp. 55–120.
Gail H.-P. and Sedlmayr E. 1998. Inorganic dust formation in astrophysical environments. *Faraday Discussions* 109:303–319.
Gail H.-P. and Sedlmayr E. 1999. Mineral formation in stellar winds: I. Condensation sequence of silicate and iron grains in stationary oxygen rich outflows. *Astronomy and Astrophysics* 347:594–616.
Gail H.-P., Zhukovska S. V., Hoppe P., and Trieloff M. 2009. Stardust from asymptotic giant branch stars. *The Astrophysical Journal* 698:1136–1154.
Gehrels N. 1986. Confidence limits for small in astrophysical data. *The Astrophysical Journal* 303:336–346.
Gobrecht D., Cherchneff I., and Sarangi A. 2015. Dust formation in the inner wind of the oxygen-rich AGB star IK Tau. In *ASP Conference Series 497*, edited by Kerschbaum F., Wing R. F., and Hron J. San Francisco, California: Astronomical Society of the Pacific. pp. 321–326.
Grossman J. N., Rubin A. E., Nagahara H., and King E. A.. 1988. Properties of chondrules. In *Meteorites and the early solar system*, edited by Kerridge J. F. and Matthews M. S. Tucon, Arizona: University of Arizona Press, pp. 680–696.
Gyngard F., Zinner E., Nittler L. R., Morgand A., Stadermann F. J., and Hynes K. M. 2010. Automated NanoSIMS measurements of spinel stardust from the Murray meteorite. *The Astrophysical Journal* 717:107–120.
Gyngard F., Nittler L. R., Zinner E., José J., and Cristallo S.. 2011. New reaction rates and implications for nova nucleosynthesis and presolar grains (abstract #2675). 42nd Lunar and Planetary Science Conference. CD-ROM.
Haack H., Grau T., Bischoff A., Horstmann M., Wasson J., Sørensen A., Laubenstein M., Ott U., Palme H., Gellissen M., Greenwood R. C., Pearson V. K., Franchi I. A., Gabelica Z., and Schmitt-Kopplin P. 2012. Maribo—A new CM fall from Denmark. *Meteoritics & Planetary Science* 47:30–50.
Haenecour P., Floss C., Zega T. J., Croat T. K., Wang A., Jolliff B. L., and Carpenter P. 2018. Presolar silicates in the matrix and fine-grained rims around chondrules in primitive CO3.0 chondrites: Evidence for pre-accretionary aqueous alteration of the rims in the solar nebula. *Geochimica et Cosmochimica Acta* 221:379–405.
Hanna R. D. and Ketcham R. A. 2018. Evidence for accretion of fine-grained rims in a turbulent nebula for CM Murchison. *Earth and Planetary Science Letters* 481:201–211.
Hanowski N. and Brearley A. J. 2000. Iron-rich aureoles in the CM carbonaceous chondrites Murray, Murchison, and Allan Hills 81002: Evidence for in situ aqueous alteration. *Meteoritics & Planetary Science* 35:1291–1308.
Hanowski N. and Brearley A. J. 2001. Aqueous alteration of chondrules in the CM carbonaceous chondrite, Allan Hills 81002: Implications for parent-body alteration. *Geochimica et Cosmochimica Acta* 65:495–518.
Harries D. and Zolensky M. E. 2016. Mineralogy of iron sulfides in CM1 and CI1 lithologies of the Kaidun breccia: Records of extreme to intense hydrothermal alteration. *Meteoritics & Planetary Science* 51:1096–1109.
Heck P. R., Floss C., and Davis A. M. 2014. Stardust in the Sutter's Mill meteorite. *Meteoritics & Planetary Science* 48:5070.
Hewins R. H., Bourot-Denise M., Zanda B., Leroux H., Barrat J.-A., Humayun M., Göpel C., Greenwood R. C., Franchi I. A., Pont S., Lorand J.-P., Cournède C., Gattacceca J., Rochette P., Kuga M., Marrocchi Y., and Marty B. 2014. The Paris meteorite, the least altered CM chondrite so far. *Geochimica et Cosmochimica Acta* 124:190–222.
Hillion F., Kilburn M. R., Hoppe P., Messenger S., and Weber P. K. 2008. The effect of QSA on S, C, O and Si isotopic ratio measurements (abstract). *Geochimica et Cosmochimica Acta* 72:A377.
Hopp T. and Vollmer C. 2018. Chemical composition and iron oxidation state of amorphous matrix silicates in the carbonaceous chondrite Acfer 094. *Meteoritics & Planetary Science* 53:153–166.

Hoppe P. and Ott U. 1997. Mainstream silicon carbide grains from meteorites. In *Astrophysical implications of the laboratory study of presolar materials*, edited by Bernatowicz T. J. and Zinner E. New York: American Institute of Physics. pp. 27–58.

Hoppe P., Leitner J., Gröner E., Marhas K. K., Meyer B. S., and Amari S. 2010. NanoSIMS studies of small presolar SiC grains: New insights into supernova nucleosynthesis, chemistry, and dust formation. *The Astrophysical Journal* 719:1370–1384.

Hoppe P., Cohen S., and Meibom A. 2013. NanoSIMS: Technical aspects and applications in cosmochemistry and biological geochemistry. *Geostandards and Geoanalytical Research* 37:111–154.

Hoppe P., Leitner J., and Kodolányi J. 2015. New constraints on the abundances of silicate and oxide stardust from supernovae in the Acfer 094 meteorite. *The Astrophysical Journal* 808:L9–L15.

Hoppe P., Leitner J., and Kodolányi J. 2017. The stardust abundance in the local interstellar cloud at the birth of the solar system. *Nature Astronomy* 1:617–620.

Howard K. T., Alexander C. M. O'D., Schrader D. L., and Dyl K. A. 2015. Classification of hydrous meteorites (CR, CM and C2 ungrouped) by phyllosilicate fraction: PSD-XRD modal mineralogy and planetesimal environments. *Geochimica et Cosmochimica Acta* 149:206–222.

Hua X., Wang J., and Buseck P. R. 2002. Fine-grained rims in the Allan Hills 81002 and Lewis Cliff 90500 CM2 meteorites: Their origin and modification. *Meteoritics & Planetary Science* 37:229–244.

Huss G. R., Fahey A. J., Gallino R., and Wasserburg G. J. 1994. Oxygen isotopes in circumstellar Al_2O_3 grains from meteorites and stellar nucleosynthesis. *The Astrophysical Journal* 430:L81–L84.

Huss G. R., Hutcheon I. D., and Wasserburg G. J. 1997. Isotopic systematics of presolar silicon carbide from the Orgueil (CI) chondrite: Implications for solar system formation and stellar nucleosynthesis. *Geochimica et Cosmochimica Acta* 61:5117–5148.

Huss G. R., Meshik A. P., Smith J. B., and Hohenberg C. M. 2003. Presolar diamond, silicon carbide, and graphite in carbonaceous chondrites: Implications for thermal processing in the solar nebula. *Geochimica Cosmochimica Acta* 67:4823–4848.

Hutcheon I. D., Huss G. R., Fahey A. J., and Wasserburg G. J. 1994. Extreme ^{26}Mg and ^{17}O enrichments in an Orgueil corundum: Identification of a presolar oxide grain. *The Astrophysical Journal* 425:L97–L100.

Jenniskens P., Fries M. D., Yin Q.-Z., Zolensky M., Krot A. N., Sandford S. A., Sears D., Beauford R., Ebel D. S., Friedrich J. M., Nagashima K., Wimpenny J., Yamakawa A., Nishiizumi K., Hamajima Y., Caffee M. W., Welten K. C., Laubenstein M., Davis A. M., Simon S. B., Heck P. R., Young E. D., Kohl I. E., Thiemens M. H., Nunn M. H., Mikouchi T., Hagiya K., Ohsumi K., Cahill T. A., Lawton J. A., Barnes D., Steele A., Rochette P., Verosub K. L., Gattacceca J., Cooper G., Glavin D. P., Burton A. S., Dworkin J. P., Elsila J. E., Pizzarello S., Ogliore R., Schmitt-Kopplin P., Harir M., Hertkorn N., Verchovsky A., Grady M., Nagao K., Okazaki R., Takechi H., Hiroi T., Smith K., Silber E. A., Brown P. G., Albers J., Klotz D., Hankey M., Matson R., Fries J. A., Walker R. J., Puchtel I., Lee C.-T. A., Erdman M. E., Eppich G. R., Roeske S., Gabelica Z., Lerche M., Nuevo M., Girten B., and Worden S. P., (the Sutter's Mill Meteorite Consortium). 2012. Radar-enabled recovery of the Sutter's Mill meteorite, a carbonaceous chondrite regolith breccia. *Science* 338:1583–1587.

Jeong K. S., Winters J. M., Le Bertre T., and Sedlmayr E. 2003. Self-consistent modeling of the outflow from the O-rich Mira IRC –20197. *Astronomy and Astrophysics* 407:191–206.

Jones A. P. 2000. Depletion patterns and dust evolution in the interstellar medium. *Journal of Geophysical Research* 105:10,257–10,268.

Jones R. H. and Rubie D. C. 1991. Thermal histories of CO3 chondrites: Application of olivine diffusion modelling to parent body metamorphism. *Earth and Planetary Science Letters* 106:73–86.

Karovicova I., Wittkowski M., Ohnaka K., Boboltz D. A., Fossat E., and Scholtz M. 2013. New insights into the dust formation of oxygen-rich AGB stars. *Astronomy and Astrophysics* 560:A75.

Keller L. P. and Messenger S. 2011. On the origins of GEMS grains. *Geochimica et Cosmochimica Acta* 75:5336–5365.

Kemper F., Waters L. B. F. M., de Koter A., and Tielens A. G. G. M. 2001. Crystallinity versus mass-loss rate in asymptotic giant branch stars. *Astronomy and Astrophysics* 369:132–141.

King A. J., Russell S. S., Schofield P. F., Humphreys-Williams E. R., Strekopytov S., Abernethy F. A. J., Verchovsky A. B., and Grady M. M. 2019. The alteration history of the Jbilet Winselwan CM carbonaceous chondrite: An analog for C-type asteroid sample return. *Meteoritics & Planetary Science* 54:521–543.

Koch I. and Floss C. 2017. Abundances and compositions of presolar grains in CR2 chondrite EET 92042 (abstract #2984). 48th Lunar and Planetary Science Conference. CD-ROM.

Kodólanyí J., Hoppe P., Gröner E., Pauly C., and Mücklich F. 2014. The Mg isotope composition of presolar silicate grains from red giant stars. *Geochimica et Cosmochimica Acta* 140:577–605.

Krestina N., Hsu W., and Wasserburg G. J. 2002. Circumstellar oxide grains in ordinary chondrites and their origin (abstract #1425) 33rd Lunar and Planetary Science conference. CD-ROM.

Lattanzio J. C. and Boothroyd A. I. 1997. Nucleosynthesis of elements in low to intermediate mass stars through the AGB phase. *AIP Conference Proceedings* 402:85–114.

Lauretta D. S., Hua X., and Buseck P. R. 2000. Mineralogy of fine-grained rims in the ALH 81002 CM chondrite. *Geochimica et Cosmochimica Acta* 64:3263–3273.

Lefèvre G., Duc M., Lepeut P., Caplain R., and Fédoroff M. 2002. Hydration of γ-alumina in water and its effects on surface reactivity. *Langmuir* 18:7530–7537.

Le Guillou C., Changela H. G., and Brearley A. J. 2015. Widespread oxidized and hydrated amorphous silicates in CR chondrites matrices: Implications for alteration conditions and H_2 degassing of asteroids. *Earth and Planetary Science Letters* 420:162–173.

Leitner J. and Hoppe P. 2019. A new population of dust from stellar explosions among meteoritic stardust. *Nature Astronomy* 3:725–729.

Leitner J., Vollmer C., Hoppe P., and Zipfel J. 2012a. Characterization of presolar material in the CR chondrite Northwest Africa 852. *The Astrophysical Journal* 745:38–53.

Leitner J., Kodolányi J., Hoppe P., and Floss C. 2012b. Laboratory analysis of presolar silicate stardust from a nova. *The Astrophysical Journal* 754:L41–L46.

Leitner J., Hoppe P., and Zipfel J. 2012c. The stardust inventories of Graves Nunataks 95229 and Renazzo: Implications for the distribution of presolar grains in CR chondrites (abstract #1835). 43rd Lunar and Planetary Science Conference. CD-ROM.

Leitner J., Metzler K., Vollmer C., and Hoppe P. 2013. Search for presolar grains in fine-grained chondrule rims: First results from CM chondrites and Acfer 094 (abstract #2273). 44th Lunar and Planetary Science Conference. CD-ROM.

Leitner J., Hoppe P., Metzler K., Vollmer C., and Zipfel J. 2014. Characterization of presolar stardust in fine-grained chondrule rims from primitive meteorites. Goldschmidt Abstracts, 2014 1400.

Leitner J., Hoppe P., Metzler K., Haenecour P., Floss C., and Vollmer C. 2015. The presolar grain inventory of CM chondrites. *Meteoritics & Planetary Science* 50:5178.

Leitner J., Vollmer C., Floss C., Zipfel J., and Hoppe P. 2016. Ancient stardust in fine-grained chondrule dust rims from carbonaceous chondrites. *Earth and Planetary Science Letters* 434:117–128.

Leitner J., Hoppe P., and Zipfel J. 2018. A study of presolar material in hydrated lithic clasts from metal-rich carbonaceous chondrites. *Meteoritics & Planetary Science* 53:204–231.

Lewis R. S., Tang M., Wacker J. F., Anders E., and Steel E. 1987. Interstellar diamonds in meteorites. *Nature* 326:160–162.

Liebig B. and Liu M. C. 2014. A Search for presolar grains in the Murchison meteorite (abstract #1631). 45th Lunar and Planetary Science Conference. CD-ROM.

Liffman K. and Toscano M. 2000. Chondrule fine-grained mantle formation by hypervelocity impact of chondrules with dusty gas. *Icarus* 143:106–125.

Lin Y., Gyngard F., and Zinner E. 2010. Isotopic analysis of supernova SiC and Si_3N_4 grains from the Qingzhen (EH3) chondrite. *The Astrophysical Journal* 709:1157–1173.

Lindgren P., Hanna R. D., Dobson K. J., Tomkinson T., and Lee M. R. 2015. The paradox between low shock-stage and evidence for compaction in CM carbonaceous chondrites explained by multiple low-intensity impacts. *Geochimica et Cosmochimica Acta* 148:159–178.

Liu N., Nittler L. R., Pignatari M., Alexander C. M. O'D., and Wang J. 2017a. Stellar origin of ^{15}N-rich presolar SiC grains of type AB: Supernovae with explosive hydrogen burning. *The Astrophysical Journal* 842:L1–L9.

Liu N., Stephan T., Boehnke P., Nittler L. R., Alexander C. M. O'D., Wang J., Davis A. M., Trappitsch R., and Pellin M. 2017b. J-type carbon stars: A dominant source of ^{14}N-rich presolar SiC grains of type AB. *The Astrophysical Journal* 844:L12–L18.

Lodders K. 2003. Solar system abundances and condensation temperatures of the elements. *The Astrophysical Journal* 591:1220–1247.

Lugaro M., Davis A. M., Gallino R., Pellin M. J., Straniero O., and Käppeler F. 2003. Isotopic compositions of strontium, zirconium, molybdenum, and barium in single presolar SiC grains and asymptotic giant branch stars. *The Astrophysical Journal* 593:486–508.

Lugaro M., Karakas A. I., Bruno C. G., Aliotta M., Nittler L. R., Bemmerer D., Best A., Boeltzig A., Broggini C., Caciolli A., Cavanna F., Ciani G. F., Corvisiero P., Davinson T., Depalo R., Di Leva A., Elekes Z., Ferraro F., Formicola A., Zs F., Gervino G., Guglielmetti A., Gustavino C., Gy G., Imbriani G., Junker M., Menegazzo R., Mossa V., Pantaleo F. R., Piatti D., Prati P., Scott D. A., Straniero O., Strieder F., Szücs T., Takács M. P., and Trezzi D. 2017. Origin of meteoritic stardust unveiled by a revised proton-capture rate of ^{17}O. *Nature Astronomy* 1:0027.

Marhas K. K., Hoppe P., Stadermann F. J., Floss C., and Lea A. S. 2006. The distribution of presolar grains in CI and CO meteorites (abstract #1959). 37th Lunar and Planetary Science Conference. CD-ROM.

Mathis J. S., Rumpl W., and Nordsieck K. H. 1977. The size distribution of interstellar grains. *The Astrophysical Journal* 217:425–433.

McSween H. Y. and Richardson S. M. 1977. The composition of carbonaceous chondrite matrix. *Geochimica et Cosmochimica Acta* 41:1145–1161.

Messenger S., Keller L. P., Stadermann F. J., Walker R. M., and Zinner E. 2003. Samples of stars beyond the solar system: Silicate grains in interplanetary dust. *Science* 300:105–108.

Messenger S., Keller L. P., and Lauretta D. S. 2005. Supernova olivine from cometary dust. *Science* 309:737–741.

Metzler K., Bischoff A., and Stöffler D. 1992. Accretionary dust mantles in CM chondrites: Evidence for solar nebula processes. *Geochimica et Cosmochimica Acta* 56:2873–2897.

Min M., Water L. B. F. M., de Koter A., Hovenier J. W., Keller L. P., and Markwick-Kemper F. 2007. The shape and composition of interstellar silicate grains. *Astronomy and Astrophysics* 462:667–676.

Mostefaoui S. and Hoppe P. 2004. Discovery of abundant in situ silicate and spinel grains from red giant stars in a primitive meteorite. *The Astrophysical Journal* 613:L149–L152.

Mostefaoui S. 2011. The search for presolar oxides in Paris. *Meteoritics & Planetary Science* 46:5170.

Nagashima K., Krot A. N., and Yurimoto H. 2004. Stardust silicates from primitive meteorites. *Nature* 428:921–924.

Nagashima K., Sakamoto N., and Yurimoto H. 2005. Destruction of presolar silicates by aqueous alteration observed in Murchison CM2 chondrite (abstract #1671). 36th Lunar and Planetary Science Conference. CD-ROM.

Nakamura T. 2005. Post-hydration thermal metamorphism of carbonaceous chondrites. *Journal of Mineralogical and Petrological Sciences* 100:260–272.

Newton J., Bischoff A., Arden W., Franchi I. A., Geiger T., Greshake A., and Pillinger C. T. 1995. Acfer 094, a uniquely primitive carbonaceous chondrite from the Sahara. *Meteoritics* 30:47–56.

Nguyen A. N. and Messenger S. 2014. Resolving the stellar sources of isotopically rare presolar silicate grains through Mg and Fe isotopic analyses. *The Astrophysical Journal* 784:149–163.

Nguyen A. N. and Zinner E. 2004. Discovery of ancient silicate stardust in a meteorite. *Science* 303:1496–1499.

Nguyen A., Zinner E., and Lewis R. S. 2003. Identification of small presolar spinel and corundum grains by isotopic raster imaging. *Publications of the Astronomical Society of Australia* 20:382–388.

Nguyen A., Stadermann F. J., Zinner E., Stroud R. M., Alexander C. M. O. D., and Nittler L. R. 2007.

Characterization of presolar silicate and oxide grains in primitive carbonaceous chondrites. *The Astrophysical Journal* 656:1223–1240.

Nguyen A. N., Nittler L. R., Stadermann F. J., Stroud R. M., and Alexander C. M. O'D. 2010. Coordinated analyses of presolar grains in the Allan Hills 77307 and Queen Elizabeth Range 99177 meteorites. *The Astrophysical Journal* 719:166–189.

Nguyen A. N., Nittler L. R., Alexander C. M. O'D., and Hoppe P. 2018. Titanium isotopic compositions of rare presolar SiC grain types from the Murchison meteorite. *Geochimica et Cosmochimica Acta* 221:162–181.

Nittler L. R. 2009. On the mass and metallicity distributions of the parent AGB stars of O-rich presolar stardust grains. *Publications of the Astronomical Society of Australia* 26:271–277.

Nittler L. R. 2019. Isotopic Imprints of Super-AGB Stars and their Supernovae in the solar system. *Meteoritics & Planetary Science* 54:6424.

Nittler L. R. and Alexander C. M. O'D. 1999. Automatic identification of presolar Al- and Ti-rich oxide grains from ordinary chondrites (abstract #2041). 30th Lunar and Planetary Science Conference. CD-ROM.

Nittler L. R. and Alexander C. M. O'D. 2003. Chromium-bearing presolar oxide grains in a ^{54}Cr-rich Orgueil residue. *Meteoritics & Planetary Science* 38:A129.

Nittler L. R. and Hoppe P. 2005. Are presolar silicon carbide grains from novae actually from supernovae? *The Astrophysical Journal*. 631:L89–L92.

Nittler L. R., Walker R. M., Zinner E., Hoppe P., and Lewis R. S. 1993. Identification of an interstellar oxide grain from the Murchison meteorite by ion imaging (abstract #1087). 24th Lunar and Planetary Science Conference. CD-ROM.

Nittler L. R., Alexander C. M. O'D., Gao X., Walker R. M., and Zinner E. K. 1994. Interstellar oxide grains from the Tieschitz ordinary chondrite. *Nature* 370:443–446.

Nittler L. R., Hoppe P., Alexander C. M. O'D., Amari S., Eberhardt P., Gao X., Lewis R. S., Strebel R., Walker R. M., and Zinner E. 1995. Silicon nitride from supernovae. *The Astrophysical Journal* 453:L25–L28.

Nittler L. R., Alexander C. M. O. D., Gao X., Walker R. M., and Zinner E. 1997. Stellar sapphires: The properties and origins of presolar Al_2O_3 in meteorites. *The Astrophysical Journal* 483:475–495.

Nittler L. R., Alexander C. M. O'D., Wang J., and Gao X. 1998. Meteoritic oxide grain from supernova found. *Nature* 393:222.

Nittler L. R., Alexander C. M. O'D., Gallino R., Hoppe P., Nguyen A. N., Stadermann F. J., and Zinner E. K. 2008. Aluminum-, calcium- and titanium-rich oxide stardust in ordinary chondrite meteorites. *The Astrophysical Journal* 682:1450–1478.

Nittler L. R., Wang J., and Alexander C. M. O'D. 2012. Confirmation of extreme ^{54}Cr enrichments in Orgueil nano-oxides and correlated O-isotope measurements (abstract #2442). 43rd Lunar and Planetary Science Conference. CD-ROM.

Nittler L. R., Alexander C. M. O'D., Davidson J., Riebe M. E. I., Stroud R. M., and Wang J. 2018. High abundances of presolar grains and ^{15}N-rich organic matter in CO3.0 chondrite Dominion Range 08006. *Geochimica et Cosmochimica Acta* 226:107–131.

Nittler L. R., Stroud R. M., Trigo-Rodríguez J. M., De Gregorio B. T., Alexander C. M. O'D., Davidson J., Moyano-Cambero C. E., and Tanbakouei S. 2019. A cometary building block in a primitive asteroidal meteorite. *Nature Astronomy* 3:659–666.

Nollett K. M., Busso M., and Wasserburg G. J. 2003. Cool bottom processes on the thermally pulsing asymptotic giant branch and the isotopic composition of circumstellar dust grains. *The Astrophysical Journal* 582:1036–1058.

Nuth J. A., Hallenbeck S. L., and Rietmeijer F. J. M. 2000. Laboratory studies of silicate smokes: Analog studies of circumstellar materials. *Journal of Geophysical Research* 105:10,387–10,396.

Ong W. J. and Floss C. 2015. Iron isotopic measurements in presolar silicate and oxide grains from the Acfer 094 ungrouped carbonaceous chondrite. *Meteoritics & Planetary Science* 50:1392–1407.

Palmerini S., La Cognata M., Cristallo S., and Busso M. 2011. Deep mixing in evolved stars. I. The effect of reaction rate revisions from C to Al. *The Astrophysical Journal* 729:3–23.

Pignatari M., Herwig F., Hirschi R., Bennett M., Rockefeller G., Fryer C., Timmes F. X., Ritter C., Heger A., Jones S., Battino U., Dotter A., Trappitsch R., Diehl S., Frischknecht U., Hungerford A., Magkotsios G., Travaglio C., and Young P. 2016. NuGrid stellar data set. I. Stellar yields from H to Bi for stars with metallicities $Z = 0.02$ and $Z = 0.01$. *The Astrophysical Journal Supplement Series* 225:24–77.

Rauscher T., Heger A., Hoffman R. D., and Woosley S. E. 2002. Nucleosynthesis in massive stars with improved nuclear and stellar physics. *The Astrophysical Journal* 576:323–348.

Rho J., Kozasa T., Reach W. T., Smith J. D., Rudnick L., DeLaney T., Ennis J. A., Gomez H., and Tappe A. 2008. Freshly formed dust in the cassiopeia a supernova remnant as revealed by the spitzer space telescope. *The Astrophysical Journal* 673:271–282.

Rho J., Reach W. T., Tappe A., Rudnick L., Kozasa T., Hwang U., Andersen M., Gomez H., DeLaney T., Dunne L., and Slavin J. 2009. Dust formation observed in young supernova remnants with spitzer. In *ASP Conference Series 414, Cosmic Dust: Near and Far*, edited by Henning T., Grün E. and Steinacker J. San Francisco, CA: ASP, p. 22.

Rietmeijer F. J. M., Nuth J. A., and Karner J. M. 1999. Metastable eutectic condensation in a Mg-Fe-SiO-H_2-O_2 vapor: Analogs to circumstellar dust. *The Astrophysical Journal* 527:395–404.

Rubin A. E., Trigo-Rodríguez J. M., Huber H., and Wasson J. T. 2007. Progressive aqueous alteration of CM carbonaceous chondrites. *Geochimica et Cosmochimica Acta* 71:2361–2382.

Russell S. S., Ott U., Alexander C. M. O'D., Zinner E. K., Arden J. W., and Pillinger C. T. 1997. Presolar silicon carbide from the Indarch (EH4) meteorite: Comparison with silicon carbide populations from other meteorite classes. *Meteoritics & Planetary Science* 32:719–732.

Ruzicka A., Grossman J. N., and Garvie L. 2014. The Meteoritical Bulletin, No. 100. *Meteoritics & Planetary Science* 49:E1–E101.

Ruzicka A., Grossman J., Bouvier A., Herd C. D. K., and Agee C. B. 2015. The Meteoritical Bulletin, No. 102. *Meteoritics & Planetary Science* 50:F1–F248.

Schmidt D. R., Woolf N. J., Zega T. J., and Ziurys L. M. 2018. Extreme ^{13}C, ^{15}N and ^{17}O isotopic enrichment in the young planetary nebula K4-47. *Nature* 564:378–381.

Schrader D. L. and Davidson J. 2017. CM and CO chondrites: A common parent body or asteroidal neighbors? Insights from chondrule silicates. *Geochimica et Cosmochimica Acta* 214:157–171.

Sears D. W. G., Benoit P. H., and Jie L. 1993. Two chondrule groups each with distinctive rims in Murchison recognized by cathodoluminescence. *Meteoritics* 28:669–675.

Simon S. B., Yoneda S., Grossman L., and Davis A. M. 1994. A $CaAl_4O_7$-bearing refractory spherule from Murchison: Evidence for very high-temperature melting in the solar nebula. *Geochimica et Cosmochimica Acta* 58:1937–1949.

Slodzian G., Hillion F., Stadermann F. J., and Zinner E. 2004. QSA influences on isotopic ratio measurements. *Applied Surface Science* 231–232:874–877.

Stadermann F. J., Floss C., and Wopenka B. 2006. Circumstellar aluminum oxide and silicon carbide in interplanetary dust particles. *Geochimica et Cosmochimica Acta* 70:6168–6179.

Stadermann F. J., Floss C., Bose M., and Lea A. S. 2009. The use of Auger spectroscopy for the in situ elemental characterization of sub-micrometer presolar grains. *Meteoritics & Planetary Science* 44:1033–1049.

Strebel R., Hoppe P., and Eberhardt P. 1997. Nitrogen, oxygen, magnesium, and titanium isotopic compositions of circumstellar oxide grains from the tieschitz and orgueil meteorites. *Meteoritics & Planetary Science* 32:A125.

Stroud R. M., Nittler L. R., and Alexander C. M. O'D. 2004. Polymorphism in presolar Al_2O_3 grains from asymptotic giant branch stars. *Science* 305:1455–1457.

Swainson I. P., Dove M. T., Schmahl W. W., and Putnis A. 1992. Neutron powder diffraction study of the akermanite-gehlenite solid solution series. *Physics and Chemistry of Minerals* 19:185–195.

Takayama A. and Tomeoka K. 2012. Fine-grained rims surrounding chondrules in the Tagish Lake carbonaceous chondrite: Verification of their formation through parent-body processes. *Geochimica et Cosmochimica Acta* 98:1–18.

Tomeoka K. and Tanimura I. 2000. Phyllosilicate-rich chondrule rims in the Vigarano CV3 chondrite: Evidence for parent-body processes. *Geochimica et Cosmochimica Acta* 64:1971–1988.

Tonui E., Zolensky M., Hiroi T., Nakamura T., Lipschutz M. E., Wang M.-S., and Okudaira K. 2014. Petrographic, chemical and spectroscopic evidence for thermal metamorphism in carbonaceous chondrites I: CI and CM chondrites. *Geochimica at Cosmochimica Acta* 126:284–306.

Trigo-Rodriguez J. M., Rubin A. E., and Wasson J. T. 2006. Non-nebular origin of dark mantles around chondrules and inclusions in CM chondrites. *Geochimica et Cosmochimica Acta* 70:1271–1290.

Verdier-Paoletti M. J., Nittler L. R., and Wang J. 2019a. First detection of presolar grains in Paris, the most preserved CM chondrite (abstract #2948). 50th Lunar and Planetary Science Conference. CD-ROM.

Verdier-Paoletti M. J., Nittler L. R., and Wang J. 2019b. High-resolution measurements of Mg, Si, Fe and Ni isotopes of O-rich presolar grains. *Meteoritics & Planetary Science* 54:6433.

Vilas F. and Gaffey M. J. 1989. Phyllosilicate absorption Features in main-belt and outer-belt asteroid reflectance spectra. *Science* 246:790–792.

Vogel N., Wieler R., Bischoff A., and Baur H. 2003. Microdistribution of primordial Ne and Ar in fine-grained rims, matrices, and dark inclusions of unequilibrated chondrites—Clues on nebular processes. *Meteoritics & Planetary Science* 38:1399–1418.

Vollmer C., Hoppe P., Brenker F. E., and Holzapfel C. 2007. Stellar MgSiO3 perovskite: A shock-transformed stardust silicate found in a meteorite. *The Astrophysical Journal* 666:L49–L52.

Vollmer C., Hoppe P., and Brenker F. E. 2008. Si isotopic compositions of presolar silicate grains from red giant stars and supernovae. *The Astrophysical Journal* 684:611–617.

Vollmer C., Hoppe P., Stadermann F. J., Floss C., and Brenker F. 2009. NanoSIMS analysis and Auger electron spectroscopy of silicate and oxide stardust from the carbonaceous chondrite Acfer 094. *Geochimica et Cosmochimica Acta* 73:7127–7149.

Vollmer C. Pelka. M., Leitner J., Janssen A., and Hoppe P. 2016. TEM investigations of amorphous silicates in fine grained rims from Antarctic CR2 chondrites (abstract #1933). 47th Lunar and Planetary Science Conference. CD-ROM.

Wasserburg G. J., Boothroyd A. I., and Sackmann I.-J. 1995. Deep circulation in red giant stars: A solution to the carbon and oxygen isotope puzzles? *The Astrophysical Journal* 447:L37–L40.

Weisberg M. K., McCoy T. J., and Krot A. N. 2006. Systematics and evaluation of meteorite classification. In *Meteorites and the early solar system II*, edited by Lauretta D. S. and McSween H. Y. Jr. Tucson, Arizona: University of Arizona Press. pp. 19–52.

Wirth R. 2004. Focused ion beam (FIB): A novel technology for advanced application of micro- and nanoanalysis in geosciences and applied mineralogy. *European Journal of Mineralogy* 16:863–876.

Yada T., Floss C., Stadermann F. J., Zinner E., Nakamura T., Noguchi T., and Lea A. S. 2008. Stardust in Antarctic micrometeorites. *Meteoritics & Planetary Science* 43:1287–1298.

Zega T. J. and Buseck P. R. 2003. Fine-grained-rim mineralogy of the Cold Bokkeveld CM chondrite. *Geochimica et Cosmochimica Acta* 67:1711–1721.

Zega T. J., Nittler L. R., Busemann H., Hoppe P., and Stroud R. M. 2007. Coordinated isotopic and mineralogic analyses of planetary materials enabled by in situ lift-out with a focused ion beam scanning electron microscope. *Meteoritics & Planetary Science* 42:1373–1386.

Zega T. J., Haenecour P., Floss C., and Stroud R. M. 2015. Circumstellar magnetite from the LAP 031117 CO3.0 chondrite. *The Astrophysical Journal* 808:55–63.

Zhao X., Floss C., Stadermann F. J., Bose M., and Lin Y. 2011. Continued investigation of presolar silicate grains in the carbonaceous chondrite Ningqiang (abstract #1982). 42nd Lunar and Planetary Science Conference. CD-ROM.

Zhao X., Floss C., Lin Y., and Bose M. 2013. Stardust investigation into the CR chondrite Grove Mountain 021710. *The Astrophysical Journal* 769:49–64.

Zhao X., Lin Y., Yin Q.-Z., Zhang J., Hao J., Zolensky M., and Jenniskens P. 2014. Presolar grains in the CM2 chondrite Sutter's Mill. *Meteoritics & Planetary Science* 49:2038–2046.

Zinner E.. 2014. Presolar grains. In *Meteorites and cosmochemical processes*, edited by Davis A. M. Amsterdam, the Netherlands: Elsevier. pp. 181–213.

Zinner E., Tang M., and Anders E. 1987. Large isotopic anomalies of Si, C, N and noble gases in interstellar

silicon carbide from the Murray meteorite. *Nature* 330:730–732.

Zinner E., Amari S., Guinness R., Nguyen A., Stadermann F. J., Walker R. M., and Lewis R. S. 2003. Presolar spinel grains from the Murray and Murchison carbonaceous chondrites. *Geochimica et Cosmochimica Acta* 67:5083–5095.

Zinner E., Nittler L. R., Hoppe P., Gallino R., Straniero O., and Alexander C. M. O'D. 2005. Oxygen, magnesium and chromium isotopic ratios of presolar spinel grains. *Geochimica et Cosmochimica Acta* 69:4149–4165.

Zinner E., Nittler L. R., Gallino R., Karakas A. I., Lugaro M., Straniero O., and Lattanzio J. C. 2006. Silicon and carbon isotopic ratios in AGB stars: SiC grain data, models, and the galactic evolution of the Si isotopes. *The Astrophysical Journal* 650:350–373.

Zolensky M., Barrett R., and Browning L. 1993. Mineralogy and composition of matrix and chondrule rims in carbonaceous chondrites. *Geochimica et Cosmochimica Acta* 57:3123–3148.

Zolensky M., Mikouchi T., Fries M., Bodnar R., Jenniskens P., Yin Q.-Z., Hagiya K., Ohsumi K., Komatsu M., Colbert M., Hanna R., Maisano J., Ketcham R., Kebukawa Y., Nakamura T., Matsuoka M., Sasaki S., Tsuchiyama A., Gounelle M., Le L., Martinez J., Ross K., and Rahman Z. 2014. Mineralogy and petrography of C asteroid regolith: The Sutter's Mill CM meteorite. *Meteoritics & Planetary Science* 49:1997–2016.

APPENDIX

Table A1. Elemental compositions of presolar silicate and oxide grains from this study determined by Auger electron spectroscopy (AES). Relative abundance errors are 3.6% (O), 11.2% (Fe), 9.4% (Mg), 11% (Si), 24.9% (Al), and 10.8% (Ca). "ol-like" stands for olivine-like grain stoichiometries ([Mg+Fe]/Si~1 and ~2), respectively. "intermed" denotes grains with intermediate (Mg+Fe)/Si ratios of ~1.3 to 1.7, while "Si-rich" and "Si-poor" characterize grains with respective ratios >2 and <1.

Grain	O (at%)	Fe (at%)	Mg (at%)	Si (at%)	Al (at%)	Ca (at%)	(Mg+Fe)/Si	Mg#[a]	Type
MUR_1B_3 left	64 ± 2	12 ± 1		24 ± 3			0.5 ± 0.1	0	Si-rich
MUR_1B_3 right	63 ± 2	18 ± 2	7 ± 1	12 ± 1			2.1 ± 0.2	28	ol-like
MRY_20_07	58 ± 2		25 ± 2	17 ± 2			1.5 ± 0.2	100	intermed
MRY_34_04	63 ± 2		9 ± 1		28 ± 7				spinel-like
MRY_34_19	64 ± 2		10 ± 1		26 ± 7				spinel-like
JW01_S4A_28	63 ± 2	18 ± 2	7.5 ± 0.7	10 ± 1		1.5 ± 0.2	2.5 ± 0.2	29	Si-poor

[a]Mg/(Mg+Fe) × 100.

Table A2. Element composition of presolar silicate grain JW01_S4A_54 determined by SEM-EDS at 5 kV acceleration voltage. Correction factors for measured element concentrations were determined from comparison of a set of standards (Yates Mine diopside, Admire olivine, bytownite) measured under the same conditions with the respective nominal compositions and applied to the measured abundances. The composition of the matrix material surrounding the grain was measured in four locations ("matrix#1" to "matrix #4") by spot analyses to allow a comparison with and dilution correction of the grain composition. The theoretical compositions of stoichiometric diopside ($MgCaSi_2O_6$) and åkermanite ($Ca_2Mg[Si_2O_7]$) are shown for comparison.

	JW01_S4A_54	dio.	åk.	matrix#1	matrix#2	matrix#3	matrix#4	Matrix average
O (at%)	60.1 ± 2.2	60	58.3	66.3 ± 1.6	64.0 ± 1.5	66.1 ± 1.5	64.9 ± 1.6	65.3 ± 1.6
Na (at%)					0.6 ± 0.2			0.2 ± 0.1
Mg (at%)	9.2 ± 0.7	10	8.3	8.3 ± 0.5	11.4 ± 0.5	11.2 ± 0.5	8.7 ± 0.5	9.9 ± 0.5
Al (at%)	1.1 ± 0.3			2.0 ± 0.3	1.3 ± 0.3	1.7 ± 0.2	2.0 ± 0.3	1.7 ± 0.3
Si (at%)	17.6 ± 1.0	20	16.7	8.9 ± 0.5	17.0 ± 0.6	14.7 ± 0.6	11.5 ± 0.6	13.0 ± 0.6
S (at%)				2.3 ± 0.5			1.7 ± 0.4	1.0 ± 0.5
Ca (at%)	11.4 ± 2.0	10	16.7					
Fe (at%)	0.7 ± 0.4			12.3 ± 0.4	5.7 ± 0.4	5.8 ± 0.4	10.2 ± 0.4	8.5 ± 0.4
Ni (at%)						0.5 ± 0.2	1.0 ± 0.3	0.4 ± 0.3
Total	100.0	100	100	100.0	100.0	100.0	100.0	100.0

dio: diopside; åk: åkermanite.

Table A3. C- and Si-isotopic compositions, sizes (determined from NanoSIMS secondary ion images), and classifications of presolar silicon carbide grains identified in Maribo, Murray, Banten, Jbilet Winselwan, and Sutter's Mill. Si-isotopic data are given as δ-values in per mil. Errors are 1 sigma.

Grain	Size (nm)	$^{12}C/^{13}C$	$\delta^{29}Si$ (‰)	$\delta^{30}Si$ (‰)	Type	Meteorite
MAR-C#-R_C1_02	525 × 490	61.2 ± 0.7	58 ± 12	60 ± 15	MS	Maribo
MAR-C#-R_C1_06a	400 × 260	78.9 ± 1.5	73 ± 11	108 ± 14	MS	Maribo
MAR-C#-R_C2_08	370 × 245	80.5 ± 1.9	2 ± 10	12 ± 12	MS	Maribo
MAR-C#-R_C2_28	395 × 290	43.1 ± 0.6	46 ± 9	51 ± 11	MS	Maribo
MAR-C#-R_C2_32	305 × 290	7.7 ± 0.1	20 ± 14	–7 ± 16	AB	Maribo
MAR-C#-R_C2_44	300 × 360	7.6 ± 0.1	54 ± 13	42 ± 16	AB	Maribo
MAR-C#-R_C2_66	175 × 225	54.5 ± 2.3	–6 ± 19	40 ± 24	MS	Maribo
MAR-C#-R_B_46	350 × 350	48.5 ± 1.8	78 ± 13	68 ± 16	MS	Maribo
MRY-C#19_8	190 × 260	69.6 ± 3.2	51 ± 30	64 ± 37	MS	Murray
MRY-C#19_11	525 × 280	61.2 ± 0.7	24 ± 8	41 ± 10	MS	Murray
MRY-C#34_3_1	350 × 300	6.8 ± 0.5	–1 ± 40	–49 ± 48	AB	Murray
MRY-C#34_3_2	260 × 175	49.8 ± 3.6	94 ± 46	133 ± 58	MS	Murray
JW01_SiC_S04A_39	260 × 360	58.8 ± 3.6	49 ± 35	60 ± 43	MS	Jbilet Winselwan
JW01_SiC_S04A_37	525 × 770	74.5 ± 1.1	62 ± 10	47 ± 12	MS	Jbilet Winselwan
JW01_SiC_S03_19	255 × 360	76.3 ± 1.5	111 ± 21	113 ± 25	MS	Jbilet Winselwan
JW01_SiC_S03_01	255 × 360	71.0 ± 2.2	30 ± 19	56 ± 24	MS	Jbilet Winselwan
BAN_2_76_1	285 × 285	90.2 ± 1.4	39 ± 10	60 ± 13	MS	Banten
BAN_2_76_2	265 × 350	71.5 ± 1.3	100 ± 15	109 ± 18	MS	Banten
BAN_1_10	285 × 400	44.0 ± 0.7	75 ± 15	42 ± 18	MS	Banten
SM2_4_C_1_37	450 × 480	65.7 ± 0.6	67 ± 9	62 ± 11	MS	Sutter's Mill
SM2_4_C_1_45	345 × 320	69.1 ± 1.0	28 ± 8	50 ± 9	MS	Sutter's Mill
Solar system		89.9	0	0		